

# The collective relaxation of globular clusters

Jean-Baptiste Fouvry<sup>1,2</sup> and others

<sup>1</sup> CNRS and Sorbonne Université, UMR 7095, Institut d’Astrophysique de Paris, 98 bis Boulevard Arago, F-75014 Paris, France

<sup>2</sup> Bluh Bluh

28 January 2021

## ABSTRACT

(To do.) We investigate the resonant relaxation of globular clusters, in particular the impact of induced long-range gravitating wakes.

**Key words:** Diffusion - Gravitation - Galaxies: kinematics and dynamics - Galaxies: nuclei

## 1 INTRODUCTION

(To do.) Following Weinberg (1986),

- What are our main aims in this paper?
- (1) To test theories of relaxation in spherical clusters
- (2) To determine the importance of collective effects
- (3) Prescription for  $\ell_{\max}$ ?
- (4) To emphasise how many basis functions are needed to accurately predict the BL flux on large scales

## 2 RELAXATION OF SPHERICAL STELLAR SYSTEMS

We consider a set of  $N$  stars of individual mass of  $\mu = M/N$ , with  $M$  the system’s total active mass. We assume that the system’s mean potential  $\psi$  is spherically symmetric:  $\psi = \psi(r)$ . Because of the spherical symmetry, stellar orbits in the potential  $\psi$  are each confined to a two-dimensional plane. They can therefore be characterised by their orientation (i.e. direction of their orbital angular momonetum vector) as well as two action variables

$$\mathbf{J} = (J_r, L), \quad (1)$$

with  $J_r$  the radial action, and  $L$  the norm of the angular momentum. We spell out explicitly all our conventions for the angle-action coordinates in Appendix A.

The fact that there are a finite number of stars in the system means that the exact potential of the system is not equal to  $\psi(r)$ , but instead fluctuates around  $\psi(r)$ . As a result stars, are gradually nudged to new mean-field orbits, i.e. they slowly drift to new values of  $\mathbf{J}$ . To describe this evolution statistically we introduce the total distribution function (DF),  $F_{\text{tot}} = F_{\text{tot}}(\mathbf{J})$ , defined so that  $\text{d}r\text{d}\mathbf{v}F_{\text{tot}}(\mathbf{J}(\mathbf{r}, \mathbf{v}))$  is the mass enclosed in the 6D phase space volume element  $\text{d}r\text{d}\mathbf{v}$ ; then integrating over all phase space we have  $\int \text{d}r\text{d}\mathbf{v}F_{\text{tot}} = M$ . Moreover, as shown in Hamilton et al. (2018) one can integrate out the variables corresponding to the orbital orientation and focus exclusively on the evolution of the system in the 2D  $\mathbf{J}$  space. To this end we define the reduced DF

$$F(\mathbf{J}) = 2L F_{\text{tot}}(\mathbf{J}). \quad (2)$$

The average number of stars within the phase space area element  $\text{d}\mathbf{J}$  is then equal to  $[(2\pi)^3/m]F(\mathbf{J})\text{d}\mathbf{J}$ , and the secular evolution of the phase space density is determined via the kinetic equation

$$\frac{\partial F(\mathbf{J})}{\partial t} = -\frac{\partial}{\partial \mathbf{J}} \cdot \mathbf{F}(\mathbf{J}). \quad (3)$$

The flux  $\mathbf{F}(\mathbf{J})$  tells us the speed and direction at which stars on average drift through action space. The primary job of kinetic theory is to provide an expression for  $\mathbf{F}$ .

Traditionally,  $\mathbf{F}$  is assumed to stem from two (seemingly) (Of course, a lot of things are hidden in this naive ‘seemingly’.) Indeed, let’s discuss this part, yes it is important in the context of this paper independent contributions as

$$\mathbf{F}(\mathbf{J}) = \mathbf{F}_{\text{NR}}(\mathbf{J}) + \mathbf{F}_{\text{RR}}(\mathbf{J}), \quad (4)$$

where  $\mathbf{F}_{\text{NR}}(\mathbf{J})$  captures the orbit-averaged non-resonant contributions while  $\mathbf{F}_{\text{RR}}(\mathbf{J})$  captures the contributions from the (dressed) resonant relaxation (RR). We now review in turn each of these contributions.

### 2.1 Non-Resonant Relaxation

The first contribution to relaxation is via ‘local’ two-body scattering events. (The word ‘local’ here denotes interactions that can be considered local in space and instantaneous in time, and therefore can be treated using the impulse approximation). In this case, each star undergoes a series of independent two-body encounters that result in small modifications to its velocities by some amount  $\delta\mathbf{v}$ . In particular,  $\delta\mathbf{v}$  is a function of the impact parameter  $b$  of the encounter in question. Summing up all such encounters by integrating over all possible  $b$ , converting to angle-action space and averaging over stellar orbits results in the orbit-averaged Fokker–Planck (FP) flux (Binney & Tremaine 2008, §7.4.2):

$$\mathbf{F}_{\text{NR}}(\mathbf{J}) = \mathbf{D}_1(\mathbf{J}) F(\mathbf{J}) - \frac{1}{2} \frac{\partial}{\partial \mathbf{J}} \cdot \left[ \mathbf{D}_2(\mathbf{J}) F(\mathbf{J}) \right], \quad (5)$$

where we introduced the first-order diffusion coefficient,  $\mathbf{D}_1(\mathbf{J})$ , as well as the second-order diffusion tensor,  $\mathbf{D}_2(\mathbf{J})$  as

$$\mathbf{D}_1(\mathbf{J}) = \begin{pmatrix} \langle \Delta J_r \rangle \\ \langle \Delta L \rangle \end{pmatrix}, \quad \mathbf{D}_2(\mathbf{J}) = \begin{pmatrix} \langle (\Delta J_r)^2 \rangle & \langle \Delta J_r \Delta L \rangle \\ \langle \Delta J_r \Delta L \rangle & \langle (\Delta L)^2 \rangle \end{pmatrix}. \quad (6)$$

and  $\langle \dots \rangle$  denotes the average increment of a given quantity per unit time. In practise we calculate  $\mathbf{D}_1$  and  $\mathbf{D}_2$  using the method of Bar-Or & Alexander (2016) — see Appendix C for details. We emphasise here that the FP diffusion coefficients do not involve any non-local resonance condition nor multipole expansion. As such,  $\mathbf{F}_{\text{NR}}$  is much less demanding to compute than  $\mathbf{F}_{\text{RR}}$  (see §2.2). Finally, note that the DF appearing in Eq. (5) is the reduced DF from Eq. (2) as it is proportional to the star density in  $\mathbf{J}$ -space.

### 2.1.1 The Coulomb logarithm

One drawback of the orbit -averaged FP theory is that it exhibits two divergences: one arising from stellar encounters with very small impact parameters, and one from encounters with very large impact parameters. As a result, the final answer  $\mathbf{F}_{\text{NR}}$  is necessarily proportional to the Coulomb logarithm

$$\ln \Lambda = \ln(b_{\max}/b_{\min}), \quad (7)$$

in which the minimum/maximum impact parameters  $b_{\min/\max}$  have to be prescribed by hand. The first of these is traditionally taken to be the scale of  $90^\circ$  deflections  $2G\mu/\sigma^2$  (in the absence of any softening), or by the considered softening length,  $\varepsilon$ , (as in Eq. (G3)):

$$b_{\min} = \begin{cases} \frac{2G\mu}{\sigma^2} & \text{(Newtonian interaction),} \\ \varepsilon & \text{(Softened interaction),} \end{cases} \quad (8)$$

with  $\sigma$  the cluster's velocity dispersion. Meanwhile the latter is normally taken to be roughly the scale of the system itself; a reasonable choice is

$$b_{\max} \sim b, \quad (9)$$

with  $b$  the typical length-scale of the considered cluster (e.g. the scale-length entering the isochrone potential, see below). Don't like the repeated  $b$  notation. Of course, interactions with this impact parameter can neither be thought of as local or impulsive.

## 2.2 Resonant Relaxation

The other form of relaxation to be considered here is via long-range resonant couplings. I've talked about the interaction of 'stars' here, though of course what's really going on is an interaction of stars with potential fluctuations. Star-star interactions provide an equivalent effective description of this (Rostoker). May want to modify the terminology here. More precisely, two stars with actions  $\mathbf{J}$  and  $\mathbf{J}'$  will resonate if there exist  $\mathbf{n}, \mathbf{n}' \in \mathbb{Z}^2$  such that

$$\mathbf{n} \cdot \boldsymbol{\Omega}(\mathbf{J}) - \mathbf{n}' \cdot \boldsymbol{\Omega}(\mathbf{J}') = 0. \quad (10)$$

where  $\boldsymbol{\Omega}(\mathbf{J}), \boldsymbol{\Omega}(\mathbf{J}')$  are the dynamical frequency vectors (§A). Moreover, these resonantly interacting pairs of stars should not be treated as an isolated 2-body system. Instead one must account for the fact that resonant interactions are conveyed through the 'dielectric medium' of the other  $N - 2$  stars, so that the corresponding behaviour is *collective*. In the analogous setting of an electrostatic plasma this leads to the phenomenon of Debye shielding, whereby

the Coulomb interaction between two particles is greatly diminished (screened) by collective motions of the many other particles found on scales longer than the Debye length. On the other hand, in a stellar system collective effects tend to amplify the strength of the interaction. Accounting for collective effects is equivalent to considering the stellar system to consist of a superposition of two-body resonant encounters with the Newtonian interaction potential replaced by an effective 'dressed' potential (Gilbert 1968; Hamilton 2021).

The theory that accounts for resonant interactions dressed by collective effects is the inhomogeneous Balescu–Lenard (BL) theory (Heyvaerts 2010; Chavanis 2012). When applied to spherical stellar systems, BL theory contributes a flux (Hamilton et al. 2018):

$$\mathbf{F}_{\text{RR}}(\mathbf{J}) = \sum_{\ell} \mathbf{F}_{\text{RR}}^{\ell}(\mathbf{J}), \quad = \sum_{\ell} \sum_{\mathbf{n}, \mathbf{n}'} \mathbf{n} \mathcal{F}_{\mathbf{n}\mathbf{n}'}^{\ell}(\mathbf{J}), \quad (11)$$

where  $\mathbf{n}, \mathbf{n}' \in \mathbb{Z}^2$  and  $\ell = 0, 1, 2, \dots$  is a harmonic index, and

$$\mathcal{F}_{\mathbf{n}\mathbf{n}'}^{\ell}(\mathbf{J}) \equiv \frac{\pi(2\pi)^3}{2\ell + 1} \mu \int d\mathbf{J}' J_2 J_2' |\Lambda_{\mathbf{n}\mathbf{n}'}^{\ell}(\mathbf{J}, \mathbf{J}', \mathbf{n} \cdot \boldsymbol{\Omega}(\mathbf{J}))|^2 \quad (12)$$

$$\times \delta_{\mathbf{D}}(\mathbf{n} \cdot \boldsymbol{\Omega}(\mathbf{J}) - \mathbf{n}' \cdot \boldsymbol{\Omega}(\mathbf{J}')) \left( \mathbf{n}' \cdot \frac{\partial}{\partial \mathbf{J}'} - \mathbf{n} \cdot \frac{\partial}{\partial \mathbf{J}} \right) \frac{F(\mathbf{J})}{J_2} \frac{F(\mathbf{J}')}{J_2'}$$

Here the coefficient  $\Lambda_{\mathbf{n}\mathbf{n}'}^{\ell}(\mathbf{J}, \mathbf{J}', \omega)$  captures the strength of the interaction of orbits with actions  $\mathbf{J}$  and  $\mathbf{J}'$  coupled via the resonance  $(\mathbf{n}, \mathbf{n}')$  at frequency  $\omega$ , and includes the effect of the collective amplification. We give the explicit expression for  $\Lambda_{\mathbf{n}\mathbf{n}'}^{\ell}$  in Appendix D. If this collective amplification effect can be considered negligible then the expression for  $\mathcal{F}_{\mathbf{n}\mathbf{n}'}^{\ell}$  is unchanged except that one substitutes new (frequency-*independent*) coefficients  $\Lambda_{\mathbf{n}\mathbf{n}'}^{\ell}(\mathbf{J}, \mathbf{J}')$  in place of the dressed coefficients  $\Lambda_{\mathbf{n}\mathbf{n}'}^{\ell}(\mathbf{J}, \mathbf{J}', \omega)$  — see Appendix E. In this the inhomogeneous BL flux reduces to the inhomogeneous Landau flux.

### 2.2.1 Divergence at small scales

Is  $\ell$  really the only thing we need to consider when talking about spatial scales? In the resonant theory, the spatial scale of each interaction is essentially set by the harmonic number  $\ell$ . Because of this, the resonant flux  $\mathbf{F}_{\text{RR}}$  does not suffer from a large-scale divergence: the largest scales in the problem are set by the minimum harmonic number  $\ell = 0$  from which there stems a finite contribution. However,  $\mathbf{F}_{\text{RR}}$  does still exhibit a small-scale divergence that one must heuristically cure. We now show how this divergence arises and then offer a prescription for dealing with it in practice.

We first note that from (12) we expect the flux  $\mathbf{F}_{\text{RR}}^{\ell}$  to be proportional to  $1/\ell$  for large  $\ell$ , a scaling already noticed by Weinberg (1986) in the context of resonant dynamical friction. However, it may be argued that the presence of the coefficient  $|\Lambda^{\ell}|^2$  may change this simple picture. In practice however it turns out that the scaling of  $|\Lambda^{\ell}|^2$  with  $\ell$  for  $\ell \gg 1$  is weak and so the relation  $\mathbf{F}_{\text{RR}}^{\ell} \propto 1/\ell$  is a good one. We confirm this prediction numerically in Figure 1 for the particular case of the spherical isochrone potential. In this figure we plot the value of the resonant flux<sup>1</sup>  $|\mathbf{F}_{\text{RR}}^{\ell}|$  at a particular

<sup>1</sup> Strictly speaking, for this calculation we ignored collective effects, so  $\mathbf{F}_{\text{RR}}^{\ell}$  here is the Landau flux not the BL flux. However identifying these flux is a good approximation since we are only interested in the large  $\ell$  behaviour where collective effects are unimportant.

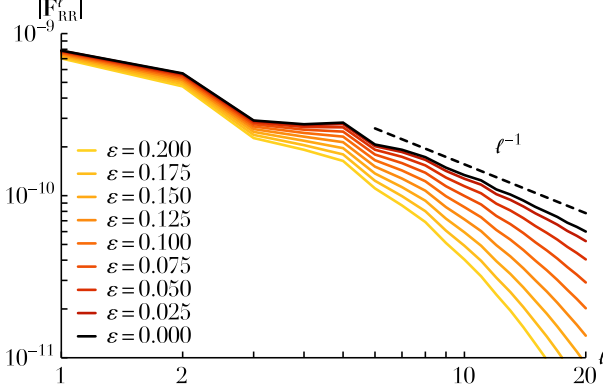


**Figure 1.** Illustration of the respective contributions from a given harmonic  $\ell$  to the resonant flux Eq. (11), in the absence of any collective effects. Here, the resonant flux has been computed at the orbital location  $(J_r, L) = (0.1, 0.5)$ , with  $0 \leq \ell \leq 20$ , and  $|n_1|, |n'_1| \leq 40$ , for various softening lengths. In particular, for the unsimplified Newtonian interaction, we recover  $|\mathbf{F}_{RR}^\ell| \propto 1/\ell$ , hence exhibiting a logarithmic divergence on small scales. The larger the softening length, the steeper the truncation of high-order harmonics, as highlighted in Eq. (E13).

phase space location  $\mathbf{J}$  as a function of  $\ell$ , and for different values of the softening parameter  $\epsilon$ . (To understand how we computed  $\mathbf{F}_{RR}^\ell$ , itself a significant technical challenge, see Appendices D–F). We see that for the purely Newtonian interaction we find the expected scaling  $|\mathbf{F}_{RR}^\ell| \propto 1/\ell$  for  $\ell \gtrsim \ell_{\text{cut}}$ , with  $\ell_{\text{cut}} = 6$ . This scaling naturally leads to a logarithmic divergence in the calculation of the RR flux, since if we treat large  $\ell \gg 1$  as a continuous variable we get a contribution  $\propto \int^{\ell_{\text{max}}} \ell \, d\ell \, \mathbf{F}^\ell \propto \int^{\ell_{\text{max}}} \ell \, d\ell / \ell \propto \ln \ell_{\text{max}}$ . The problem is therefore to choose the  $\ell_{\text{max}}$  at which the infinite harmonic sum from Eq. (11) should be truncated.

The efficiency of resonant interactions is determined by the coupling coefficients  $\Lambda_{nn'}^\ell$ . For large  $\ell$  we expect collective amplification to be unimportant as high frequency oscillation cancel out long range effects, so we consider only the bare coefficients defined in Eq. (E5). From Eq. (E4) we know that these coefficients are proportional to

$$U_\ell(r, r') \propto \frac{1}{r_{\text{max}}} \left( \frac{r_{\text{min}}}{r_{\text{max}}} \right)^\ell, \quad (13)$$

with  $r_{\text{min}} = \min(r, r')$  and  $r_{\text{max}} = \max(r, r')$ . As  $\ell$  increases, this function gets sharper so that only very local interactions get picked up. Let us then consider one such interaction in the core of the cluster, and let us take  $r_{\text{max}} = b$  (the typical lengthscale of the cluster's density), and  $r_{\text{min}} = b(1-\alpha)$ , with  $\alpha > 0$ . For two stars to have a close encounter necessarily requires that  $\alpha$  is very small. Therefore in the limit of interest ( $\alpha \ll 1, \ell \gg 1$ ), Eq. (13) becomes

$$U_\ell(\alpha) \propto \frac{1}{b} (1-\alpha)^\ell \simeq \frac{1}{b} e^{-\ell\alpha}. \quad (14)$$

The typical separation associated with this interaction is that given by its half-width, i.e. the value of  $\alpha$  such that  $U_\ell(\alpha)/U_\ell(0) = \frac{1}{2}$ . One naturally gets  $\alpha = \ln(2)/\ell$ . For a given harmonic  $\ell$ ,  $b\alpha$  then corresponds to the smallest scale of separation that is effectively resolved by the coupling coefficients. As a consequence, equating this interaction scale with  $b_{\text{min}}$ , we may then truncate the harmonics expansion at

$$\ell_{\text{max}} = \ln(2) \frac{b}{b_{\text{min}}}. \quad (15)$$

### 3 APPLICATION TO THE SPHERICAL ISOCHRONE MODEL

So far our results have been applicable to any stellar system with a spherically symmetric mean field. Hereafter we will use the isochrone potential  $\psi = -GM/(b + \sqrt{b^2 + r^2})$  with a self-consistent DF. Moreover we choose this DF to have an isotropic velocity distribution, so that  $F_{\text{tot}} = F_{\text{tot}}(E)$ . Other details of the model are given in Appendix F.

**Need a contour plot of  $F(L, J_r)$  — in particular, we need to know how much of the system we are actually considering when plotting  $L \in (0, 1)$  and  $J_r \in (0, 0.5)$ .**

(To do.)

#### 3.1 Curing divergences

**missing a transition** For the particular case  $N = 10^5$ , and the parameters considered in our numerical simulations (see Appendix G) we readily find from Eqs. (G1) and (G6) that the classical Coulomb logarithm reads

$$\ln \Lambda \simeq \begin{cases} 8.69 & (\text{Newtonian interaction}), \\ 3.59 & (\text{Softened interaction}). \end{cases} \quad (16)$$

**(Check again these values.)** As a result, for such a large value of  $N$ , strong encounters are drastically suppressed by the softening, slowing down the evolution almost by a factor of 3. Similarly, following Eqs. (8) and (15), for our fiducial case we truncate the resonant flux computation at

$$\ell_{\text{max}} \simeq \begin{cases} 4115 & (\text{Newtonian interaction}), \\ 25 & (\text{Softened interaction}). \end{cases} \quad (17)$$

**(Check values.)** We note that the introduction of softening strongly reduces the range of harmonics that contribute to the (collisionless) dynamics.

#### 3.2 Computing the RR flux

In Fig. 1, we determined the harmonics,  $\ell_{\text{cut}}$ , at which the logarithmic scaling,  $\mathbf{F}_\ell \propto 1/\ell$ , starts to appear. In addition, in Eq. (17), we determined the maximum harmonic number,  $\ell_{\text{max}}$ , that may be considered in the infinite sum over harmonics. In practice, as illustrated in Fig. (3), for the sake of numerical feasibility, one can only estimate numerically the diffusion fluxes,  $\mathbf{F}_{RR}^\ell$ , for small enough values of  $\ell$ , e.g. for  $\ell \leq \ell_{\text{calc}}$  with  $\ell_{\text{calc}} = 11$ . Let us now detail how one may estimate the associated total diffusion flux. We write

$$\mathbf{F}_{RR} = \mathbf{F}_{RR}^{\text{low } \ell} + \kappa \mathbf{F}_{RR}^{\text{high } \ell} \quad (18)$$

In that expression, we introduced the two fluxes, associated respectively with low- and high-order harmonics

$$\mathbf{F}_{RR}^{\text{low } \ell} = \sum_{\ell=0}^{\ell_{\text{cut}}-1} \mathbf{F}_{RR}^\ell; \quad \mathbf{F}_{RR}^{\text{high } \ell} = \sum_{\ell=\ell_{\text{cut}}}^{\ell_{\text{calc}}} \mathbf{F}_{RR}^\ell, \quad (19)$$

as well as the numerical prefactor,  $\kappa$ , stemming from the logarithmic scaling, that reads

$$\kappa = \left[ \sum_{\ell=\ell_{\text{cut}}}^{\ell_{\text{max}}} 1/\ell \right] / \left[ \sum_{\ell=\ell_{\text{cut}}}^{\ell_{\text{calc}}} 1/\ell \right]. \quad (20)$$

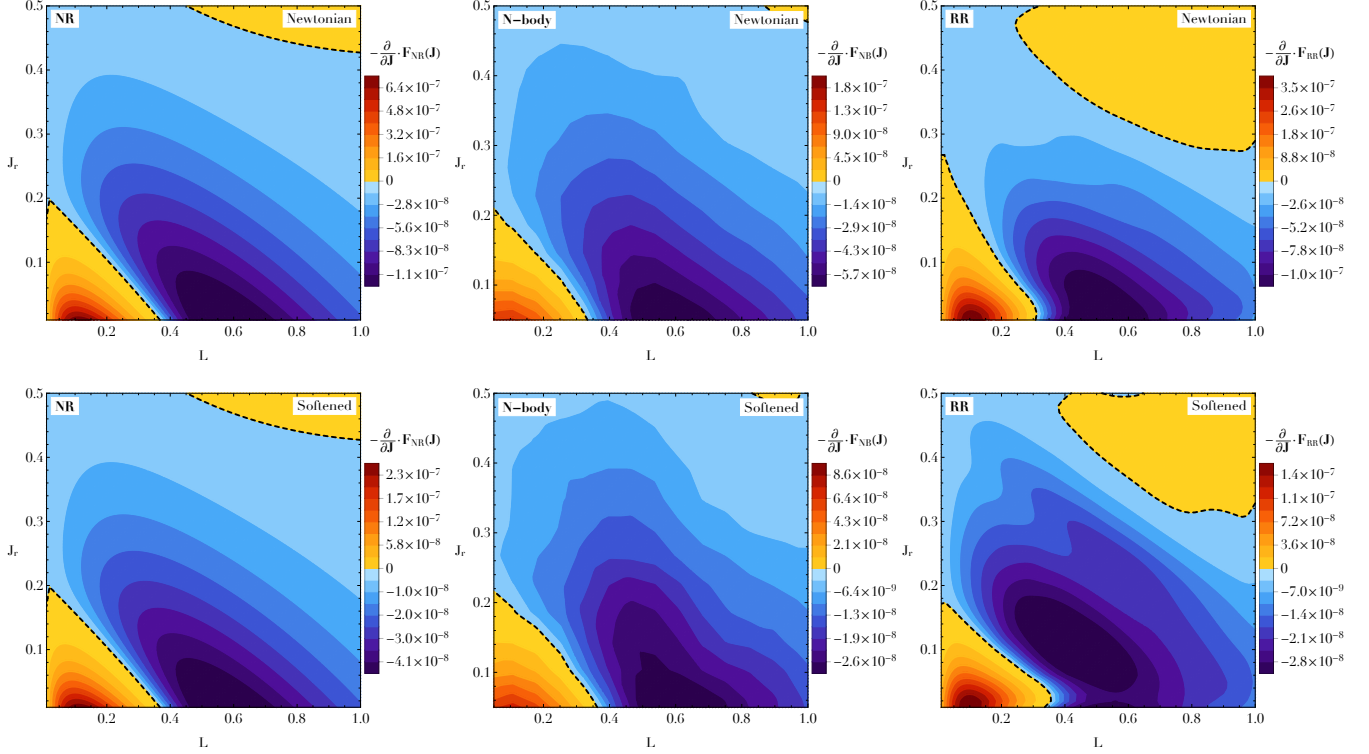


**Figure 2.** Illustration of the divergence of the diffusion flux,  $-\partial/\partial\mathbf{J} \cdot \mathbf{F}(\mathbf{J}) = \partial F/\partial t$ , as predicted by the NR theory (left), measured in numerical simulations (centre), and predicted by the RR theory (right), in units  $G=M=b=1$  [I feel strongly that the  $G, M, b$  units should be put in everywhere. Blue regions correspond to regions where the number of orbits is predicted to decrease, while red regions correspond to an increase in the number of orbits. should multiply fluxes by  $10^8$  and write  $10^8 \partial F/\partial t$  instead of flux possibly split figure in two: softened is another matter. This is the opposite convention to that used in Fouvry+ 2015 and Hamilton+ 2018! I think we should stick with the old convention. Here, the top row corresponds to a (unsoftened) Newtonian interaction, while the bottom row corresponds to a softened pairwise interaction, with their respective prescriptions to deal with the Coulomb divergence. (The N-body map does not have exactly the same range as the other ones. Should be fixed.) (Maybe for a given row, I should use the exact same color scale.) (The smoothing I perform can reduce, somewhat strongly, the values of the amplitudes.)

Definitely should have a uniform colour scale and the majority of white space removed. I can make such plots if desirable.

(Check again.) (Not sure whether the notation  $\kappa$  is ideal.) In practice, for the particular values of  $\ell_{\max}$  from Eq. (17), we obtain

$$\kappa = \begin{cases} 8.98 & \text{(Newtonian interaction),} \\ 2.08 & \text{(Softened interaction).} \end{cases} \quad (21)$$

### 3.3 Comparing RR, NR and N-body evolution

Following Eq. (18), Fig. 2 presents the total diffusion flux predicted by the RR theory. In that figure, importantly, we note that the amplitude of  $\partial F/\partial t$  matches quite well the amplitudes measured in the numerical simulations. While the shape of the contours slightly differ, note that the agreement of the amplitudes is improved compared to the NR maps [seen where?], which were over-estimated approximately by a factor 2.

Heuristically, Eq. (18) should be understood as follows. On the one hand, for  $\ell \lesssim \ell_{\text{cut}}$ , as highlighted in Eq. (13), the pairwise coupling between orbits is not yet a very sharp function of their respective separation. As a consequence, for such low-order harmonics, long-range resonant couplings are possible, leading to the diffusion maps presented in the first panels of Fig. 3. On the other hand, for  $\ell \gtrsim \ell_{\text{cut}}$ , the pairwise coupling becomes a sharp function of the stars' separations. As a consequence, for such high-order harmonics, relaxation is made possible only through local couplings,

i.e. the relaxation captured by the non-resonant theory from Eq. (5). As highlighted in the last panels of Fig. 3, this allows for the maps of  $\mathbf{F}_{\text{RR}}^{\ell}$  to greatly resemble the ones from  $\mathbf{F}_{\text{NR}}$  (see Fig. 3), up to an overall change in the amplitude, that follows the logarithmic scaling recovered in Fig. 1. As a conclusion, the main contribution from the current RR theory is to offer an improved estimation of the diffusion flux for low-order harmonics (i.e. the contributions from large scales), and subsequently offer an improved estimation of the system's appropriate  $\ln \Lambda$ . While this does not significantly affect the overall structure of the maps of  $\partial F/\partial t$ , this improves the estimation of the overall amplitude of the diffusion flux.

## 4 DISCUSSION

We have done XXX. We found that XXX.

Found collective effects to be unimportant in the dynamics of hot spherical systems, DESPITE the unarguable existence of weakly damped modes. Discuss flaws in H18 and Lau. Lau calculates only diffusion and this matches very closely the Chandra prediction. In particular, H18 didn't use anywhere near enough basis functions – moral: don't rely on a nice mode calculation ( $\ell = 2$  in my case) to believe that the code is good enough! Chandra is

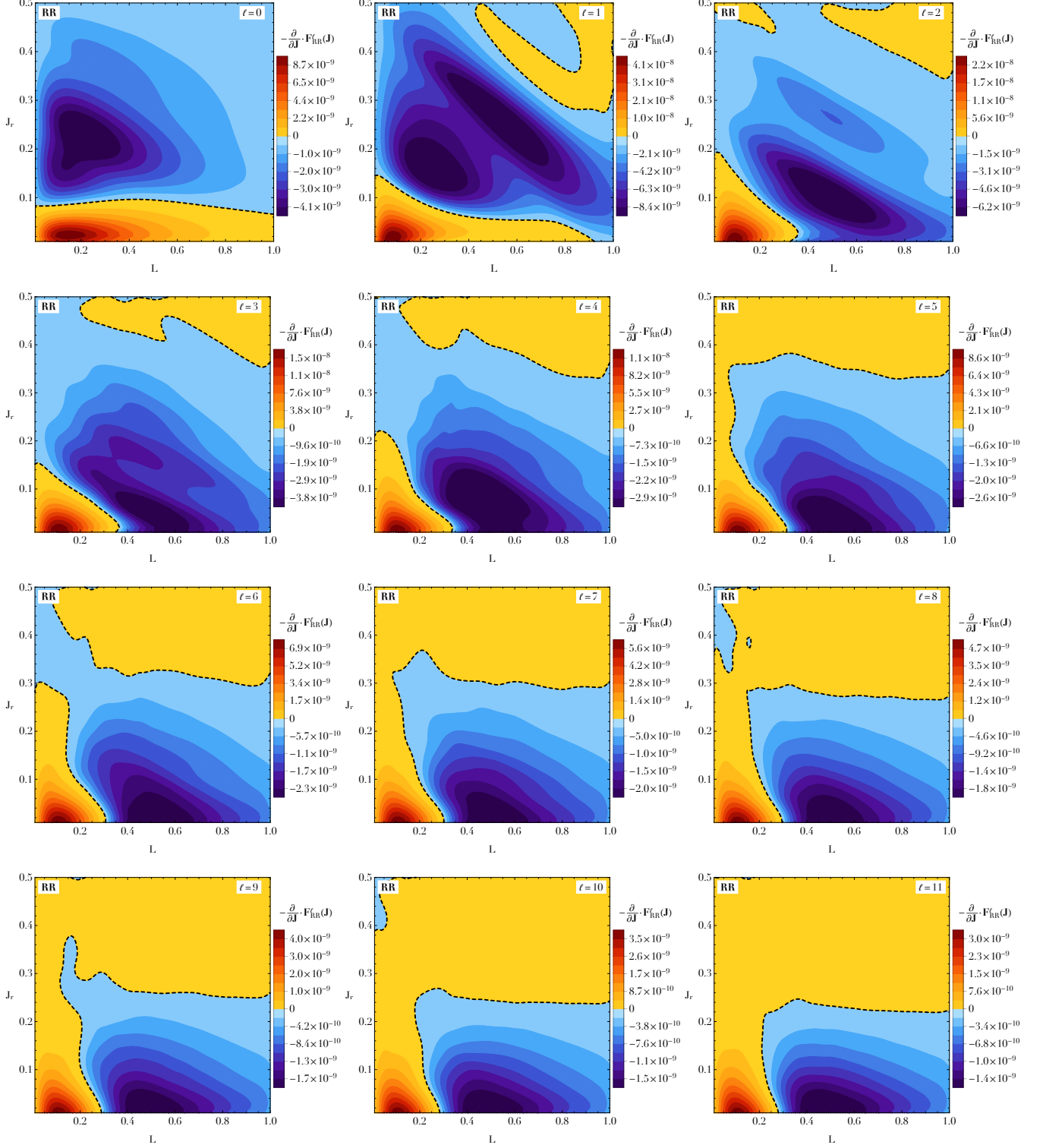


**Figure 3.** Illustration of the divergence of the bare resonant diffusion flux,  $-\partial/\partial\mathbf{J}\cdot\mathbf{F}_{\text{RR}}^{\ell}(\mathbf{J})=\partial F/\partial t$ , as defined in Eq. (11), in units  $G=M=b=1$ , as a function of the considered harmonics  $\ell$ , using the same convention as in Fig. 2. For  $\ell$  large enough, the similarities with the local predictions presented in Fig. 2 is striking. [should be in an appendix?](#)

the better effective description, but note not to take it literally since collisions at  $b \sim 1\text{pc}$  are certainly not impulsive.

(To do.)

#### 4.1 Limitations and future extensions

Of course, the present work is only a first step towards a complete description of the collective, long-range and resonant relaxation of globular clusters. Let us now briefly list venues that would deserve further investigations.

First, for the sake of simplicity, we limited ourselves to only considering isotropic **non rotating** clusters, i.e. clusters whose DF follows  $F_{\text{tot}} = F_{\text{tot}}(E)$ . As recently highlighted in Breen et al. (2017), clusters with (strong) tangential anisotropy can undergo a much more efficient relaxation. Accounting for anisotropic DFs, i.e.  $F_{\text{tot}} = F_{\text{tot}}(E, L)$ , would ask for two main developments: (i) in the NR theory, as in Eq. (C2), this asks for the computation of Rosenbluth potentials involving 2D integrals; (ii) in the RR theory, e.g. as highlighted in Rozier et al. (2019), clusters can support an ever stronger self-gravitating amplification, which may (or may not) lead to an efficient collective dressing of the low-order harmonics. Following that paper, understanding the secular relaxation of rotating spheres would also be of genuine astrophysical interest: the set of possible resonances gets shifted by rotation, and those stars can extract free energy from the mean rotation of the sphere, which may impact the importance of collective effects especially at low  $\ell$ .

Second, the present investigation was limited to the case of an isochrone potential. It was picked for the convenience of offering an explicit angular mapping, as in Eq. (F10), making the orbital averages numerically much more sound. Provided such explicit and well-behaved mappings can be designed, the present works could then naturally be extended to other cored potentials, as well as cuspy ones. In addition, we limited ourselves to only computing the divergence of the diffusion flux at the initial time,  $t=0$ . It would be of interest to use the same kinetic theories to integrate forward in time the dynamics of  $F(\mathbf{J}, t)$ , ideally up to the time of the cluster's core collapse. Given the complexity of both the NR and RR formalisms, this will be no easy task.

Third, when computing the RR flux in Fig. 3, we emphasised that for  $\ell$  large enough, the maps of  $-\partial/\partial\mathbf{J} \cdot \mathbf{F}_{\text{RR}}^\ell$  greatly resemble the one of  $-\partial/\partial\mathbf{J} \cdot \mathbf{F}_{\text{NR}}$ . From the theoretical point of view, it would then be interesting to understand in detail how a global resonance condition,  $\delta_D(\mathbf{n} \cdot \boldsymbol{\Omega} - \mathbf{n}' \cdot \boldsymbol{\Omega}')$ , between orbits, as captured by the RR theory, formally falls back on the orbit-averaged contributions from local homogeneous deflections, as captured by the NR theory.

Fourth, while it is true that the BL equation captures the amplification, and that this amplification tends to be greatest when  $\omega$  is close to the pattern frequency of a weakly damped normal mode of the stellar system, it does not account for the direct interaction between stars and this wave mode. In plasma physics the interaction between stars and waves is the subject of quasilinear (QL) theory. Recently, Hamilton & Heinemann (2020) wrote down the QL collision operator for weakly damped modes in stellar systems which accounts for these interactions. Indeed, weakly damped modes are weakly damped precisely because there are not many stars with which they resonate; hence, it may be expected that these QL interactions do not contribute much to the global evolution of  $F$ . On the other hand their slow pattern speed means that they will interact resonantly with stars which are on large, long-period orbits and therefore only weakly bound to the system. This might lead

to excess evaporation beyond the two-body prediction. However, applying the QL operator in practise as it first requires a detailed characterisation of the damped modes of a given cluster (Weinberg 1994; Heggie et al. 2020) through linear response theory.

Finally, we emphasised here that the relaxation of a star's 'in-plane' actions, i.e.  $\mathbf{J} = (J_r, L)$ , up to a correction in the Coulomb logarithm, is mainly driven by the local NR theory. Similarly, it would then be of interest to determine whether or not the relaxations of the 'out-of-plane' actions, i.e.  $\hat{\mathbf{L}}$  the instantaneous orientation of the orbital plane, is also mainly driven by NR effects, or RRones, following the steps of Meiron & Kocsis (2019); Fouvry et al. (2019).

## 5 CONCLUSION

The dynamical relaxation of globular cluster has a long history dating back to Chandrasekhar (1943). It might surprise that almost 80 years later, this topic of research should remain so active. While it has been claimed recently (Fouvry et al. 2015; Hamilton et al. 2018; Lau & Binney 2019) that collective effects are paramount to accelerating its efficiency, our present work shows that for an isotropic isochrone sphere, Chandrasekhar's orbit averaged prescription better matches taylored simulations. The dominant contribution to the fluxes arises from the decades of high harmonics which are little impacted by polarisation, whereas the impact of the wakes on the low harmonics remains modest for such a hot sphere. It will be of interest to see if this result hold for colder, rotating systems.

## ACKNOWLEDGEMENTS

This work is partially supported by the grant Segal ANR-19-CE31-0017 of the French Agence Nationale de la Recherche. We thank Stéphane Roubertol for the smooth running of the Horizon Cluster, where the simulations were performed.

## DATA AVAILABILITY

The data and numerical codes underlying this article were produced by the authors. They will be shared on reasonable request to the corresponding author.

## REFERENCES

- Bar-Or B., Alexander T., 2016, *ApJ*, 820, 129
- Binney J., Tremaine S., 2008, *Galactic Dynamics: Second Edition*. Princeton University Press
- Breen P. G., Varri A. L., Heggie D. C., 2017, *MNRAS*, 471, 2778
- Chandrasekhar S., 1943, *ApJ*, 97, 255
- Chavanis P.-H., 2012, *Physica A Statistical Mechanics and its Applications*, 391, 3680
- Dehnen W., 2000, *ApJ*, 536, L39
- Fouvry J. B., Pichon C., Magorrian J., Chavanis P. H., 2015, *A&A*, 584, A129
- Fouvry J.-B., Bar-Or B., Chavanis P.-H., 2019, *ApJ*, 883, 161
- Gilbert I. H., 1968, *The Astrophysical Journal*, 152, 1043
- Hamilton C., 2021, *Monthly Notices of the Royal Astronomical Society*, 501, 3371
- Hamilton C., Heinemann T., 2020, arXiv e-prints, p. arXiv:2011.14812
- Hamilton C., Fouvry J.-B., Binney J., Pichon C., 2018, *MNRAS*, 481, 2041
- Heggie D. C., Breen P. G., Varri A. L., 2020, *MNRAS*, 492, 6019

- Henon M., 1959, Annales d'Astrophysique, 22, 126  
 Hénon M. H., 1971, Ap&SS, 14, 151  
 Heyvaerts J., 2010, MNRAS, 407, 355  
 Kalnajs A. J., 1976, ApJ, 205, 745  
 Lau J. Y., Binney J., 2019, MNRAS, 490, 478  
 Meiron Y., Kocsis B., 2019, ApJ, 878, 138  
 Press W., et al., 2007, Numerical Recipes 3rd Edition. Cambridge Univ. Press  
 Rozier S., Fouvry J. B., Breen P. G., Varri A. L., Pichon C., Heggie D. C., 2019, MNRAS, 487, 711  
 Saha P., 1991, MNRAS, 248, 494  
 Theuns T., 1996, MNRAS, 279, 827  
 Tremaine S., Weinberg M. D., 1984, MNRAS, 209, 729  
 Wachlin F. C., Carpintero D. D., 2006, Rev. Mex. Astron. Astrofis., 42, 251  
 Wang L., Spurzem R., Aarseth S., Nitadori K., Berczik P., Kouwenhoven M. B. N., Naab T., 2015, MNRAS, 450, 4070  
 Weinberg M. D., 1986, ApJ, 300, 93  
 Weinberg M. D., 1989, MNRAS, 239, 549  
 Weinberg M. D., 1994, ApJ, 421, 481

## APPENDIX A: MEAN-FIELD DYNAMICS

In this Appendix we spell out all our conventions to describe the mean-field dynamics of a spherically symmetric 3D stellar system.

Following the notations from Tremaine & Weinberg (1984), we define the 3D angle-action coordinates as

$$\mathbf{J}_{\text{tot}} = (J_r, L, L_z), \quad (\text{A1})$$

with the associated angles  $\boldsymbol{\theta}_{\text{tot}} = (\theta_1, \theta_2, \theta_3)$ , and orbital frequencies  $\boldsymbol{\Omega}_{\text{tot}} = (\Omega_1, \Omega_2, 0)$ . In that expression,  $J_r$  is the radial action,  $L$  the norm of the angular momentum vector, and  $L_z$  its projection along the z-direction. As a result of spherical symmetry  $\Omega_3 = 0$ , because mean-field orbits remain within their orbital plane. The other two frequencies are given by

$$\begin{aligned} \frac{2\pi}{\Omega_1} &= 2 \int_{r_p}^{r_a} \frac{dr}{\sqrt{2(E - \psi(r)) - J_2^2/r^2}}, \\ \frac{\Omega_2}{\Omega_1} &= \frac{J_2}{\pi} \int_{r_p}^{r_a} \frac{dr}{r^2 \sqrt{2(E - \psi(r)) - J_2^2/r^2}}. \end{aligned} \quad (\text{A2})$$

Once the orbit has been characterised, the position of the star is obtained through the angles

$$\begin{aligned} \theta_1 &= \int_{\mathcal{C}} dr \frac{\Omega_1}{\sqrt{2(E - \psi(r)) - J_2^2/r^2}}, \\ \theta_2 - \varphi &= \int_{\mathcal{C}} dr \frac{\Omega_2 - J_2/r^2}{\sqrt{2(E - \psi(r)) - J_2^2/r^2}}, \end{aligned} \quad (\text{A3})$$

where  $\mathcal{C}$  is the contour going from the pericentre  $r_p$  up to the current position  $r = r(\theta_1)$ , along the radial oscillation. The quantity  $\varphi$  in (A3) is the angle from the ascending node to the current location of the particle along the orbital motion — see Fig. 1 of Tremaine & Weinberg (1984).

As mentioned in §2 one can take advantage of the spherical symmetry of the problem and work exclusively with the in-plane angle-action coordinates. Thus we define

$$\mathbf{J} \equiv (J_r, L); \quad \boldsymbol{\theta} \equiv (\theta_1, \theta_2); \quad \boldsymbol{\Omega} \equiv (\Omega_1, \Omega_2). \quad (\text{A4})$$

Importantly, a mean field orbit is characterised by just two quantities, the actions  $(J_r, L)$ . It will sometimes be more convenient instead to label orbits with the apo/pericentre distances  $(r_p, r_a)$ , which are related to energy  $E$ , and the angular momentum  $L$  by

$$E = \frac{r_a^2 \psi(r_a) - r_p^2 \psi(r_p)}{r_a^2 - r_p^2}; \quad L = \sqrt{\frac{2(\psi(r_a) - \psi(r_p))}{r_p^{-2} - r_a^{-2}}}. \quad (\text{A5})$$

One final way to label orbits, useful in numerical work, is via an effective semi-major axis and eccentricity defined as

$$a = \frac{r_p + r_a}{2}; \quad e = \frac{r_a - r_p}{r_a + r_p}. \quad (\text{A6})$$

## APPENDIX B: LINEAR RESPONSE THEORY

### B1 Basis method

In order to characterise the linear stability of a self-gravitating system, we follow the basis method (Kalnajs 1976). We introduce a set of potentials and densities  $(\psi^{(\alpha)}, \rho^{(\alpha)})$  that satisfy the biorthogonality relation

$$\begin{aligned} \psi^{(\alpha)}(\mathbf{r}) &= - \int d\mathbf{r}' U(\mathbf{r}, \mathbf{r}') \rho^{(\alpha)}(\mathbf{r}'), \\ \int d\mathbf{r} \psi^{(\alpha)*}(\mathbf{r}) \rho^{(\beta)}(\mathbf{r}) &= -\delta_{\alpha\beta}, \end{aligned} \quad (\text{B1})$$

with  $U(\mathbf{r}, \mathbf{r}') = -G/|\mathbf{r} - \mathbf{r}'|$  the gravitational pairwise interaction. In the case of a spherical system, it is natural to write

$$\begin{aligned} \psi^{(\alpha)}(\mathbf{r}) &= Y_\ell^m(\vartheta, \phi) U_n^\ell(r), \\ \rho^{(\alpha)}(\mathbf{r}) &= Y_\ell^m(\vartheta, \phi) D_n^\ell(r), \end{aligned} \quad (\text{B2})$$

where  $(r, \vartheta, \phi)$  are the usual spherical coordinates and  $Y_\ell^m$  are spherical harmonics normalised such that  $\int d\phi d\cos\theta |Y_\ell^m(\theta, \phi)|^2 \equiv \int d\hat{\mathbf{r}} |Y_\ell^m(\hat{\mathbf{r}})|^2 = 1$ . Eq. (B2) also involves the radial functions  $(U_n^\ell, D_n^\ell)$ , which we take to be real. As such, a given basis element is characterised by three integers: the label  $\alpha$  is a shorthand for the triplet  $(\ell, m, n)$  where  $\ell = 0, 1, 2, \dots$  and  $m = -\ell - \ell + 1, \dots, \ell$  describe the angular dependence and  $n \geq 1$  gives the radial dependence.

In practice we use as radial basis elements spherical Bessel functions (see Eq. (60) of Weinberg (1989)). With our present convention, the radial function of the potential basis elements reads

$$U_n^\ell(r) = -\frac{\sqrt{8\pi G/R_b}}{\alpha_{\ell n} |j_\ell(\alpha_{\ell n})|} j_\ell(\alpha_{\ell n} r/R_b), \quad (\text{B3})$$

where the density is assumed to vanish beyond the truncation radius  $R_b$ ,  $j_\ell$  is the spherical Bessel function of the first kind and  $\alpha_{\ell n}$  is the  $n$ -th zero of  $j_{\ell-1}$ . Then,  $D_n^\ell(r)$  is given by

$$D_n^\ell(r) = \frac{\alpha_{\ell n}}{\sqrt{2\pi G R_b^{5/2}} |j_\ell(\alpha_{\ell n})|} j_\ell(\alpha_{\ell n} r/R_b). \quad (\text{B4})$$

### B2 Response matrix

Having constructed basis elements, they may now be used to represent the potential fluctuations present in the system so as to characterise its linear stability. Following Eq. (37) of Hamilton et al. (2018), for a given harmonic  $\ell$ , the linear stability of a stellar cluster is characterised by the response matrix,  $\mathbf{M}_\ell(\omega)$  with coefficients

$$\begin{aligned} M_{pq}^\ell(\omega) &= \frac{2(2\pi)^3}{2\ell + 1} \sum_{\substack{n_1 \\ |n_2| \leq \ell \\ (\ell - n_2) \text{ even}}} |y_\ell^{n_2}|^2 \int d\mathbf{J} J_2 \frac{\mathbf{n} \cdot \partial F_{\text{tot}} / \partial \mathbf{J}}{\omega - \mathbf{n} \cdot \boldsymbol{\Omega}(\mathbf{J})} \\ &\quad \times W_{\ell p}^{\mathbf{n}}(\mathbf{J}) W_{\ell q}^{\mathbf{n}}(\mathbf{J}). \end{aligned} \quad (\text{B5})$$

Here  $y_\ell^n \equiv Y_\ell^n(\frac{\pi}{2}, 0)$  are pure numbers (while (see Eq. (34) Hamilton et al. 2018))

$$W_{\ell n}^{\mathbf{n}}(\mathbf{J}) = \int_0^\pi \frac{d\theta_1}{\pi} U_n^\ell(r) \cos(n_1 \theta_1 + n_2(\theta_2 - \psi)), \quad (\text{B6})$$

whose computation relies on the angle mappings from Eq. (A3). Having computed the response matrix, we may finally define the susceptibility matrix as

$$\mathbf{N}_\ell(\omega) = [\mathbf{I} - \mathbf{M}_\ell(\omega)]^{-1}. \quad (\text{B7})$$

This matrix characterises the amplitude of the self-gravitating dressing of potential fluctuations, and is therefore involved in the dressed resonant diffusion flux (see Eq. (D1)).

### B3 Numerical computation

The most demanding computation in Eq. (B5) is the computation of the coupling coefficients,  $W_{\ell n}^n(\mathbf{J})$ , as defined in Eq. (B6). In order to accelerate their evaluation, we follow an approach similar to the one of Appendix B of Rozier et al. (2019).

First, as already introduced in Eq. (A6), we label the orbits using  $(a, e)$ . To compute any integral, we follow the same trick as in Hénon (1971), and define an effective anomaly,  $-1 \leq u \leq 1$ , through the explicit mapping

$$r(u) = a(1 + ef(u)) \quad \text{with} \quad f(u) = u\left(\frac{3}{2} - \frac{1}{2}u^2\right). \quad (\text{B8})$$

Doing so, any integral over  $\theta_1$  can be rewritten as

$$\int_0^\pi d\theta_1 F = \int_{r_p}^{r_a} dr \frac{d\theta_1}{dr} F = \int_{-1}^1 du \frac{d\theta_1}{dr} \frac{dr}{du} F, \quad (\text{B9})$$

where the Jacobian,  $d\theta_1/dr$ , naturally follows from Eq. (A3). Following such a change of variables, integrands now have finite values at the edge of the integration domain. Furthermore, in order to increase the numerical stability of the scheme, we use an exact and well-posed expression for  $d\theta_1/du$ , as presented from Eq. (F10) for the specific case of the isochrone potential.

Following this rewriting, one could still naively interpret Eq. (B6) as involving nested integrals, since one must also compute the values of  $\theta_1[u]$  and  $(\theta_2 - \psi)[u]$  following Eq. (A3). Fortunately, we can use the same trick as in Appendix B of Rozier et al. (2019) and interpret these joint integrals simply as the forward integration of a single 3-vector. This is the approach we pursued here. In practice, we used the traditional RK4 scheme (see, e.g., Press et al. 2007), using  $K$  steps. More importantly, we used the analytical expression from Eq. (F10) that ensures that  $d\theta_1/du$  is always numerically well-behaving, preventing any issues at boundary of the integration where the radial velocity vanishes.

Having computed the coefficients  $W_{\ell n}^n(\mathbf{J}, \mathbf{J}')$ , we now have at our disposal an efficient evaluation of the integrand from Eq. (B5). In order to carry out the action integral present there, we follow the same approach as in Fouvry et al. (2015) up to three main improvements. (i) The action space,  $\mathbf{J}$ , is remapped to the dimensionless coordinates  $(x, e) = (a/b, e)$ , with  $b$  the lengthscale of the considered isochrone model. It is within these coordinates that the orbital domain is tiled in small square regions of extension  $\Delta x \times \Delta e$ . (ii) In the expression of the approximated integrands, derivatives, such as  $\partial W_{\ell n}^n / \partial x$  and  $\partial W_{\ell n}^n / \partial e$ , are not computed through finite differences but rather through their analytical expressions by computing explicitly the derivatives under the integral sign. (iii) All angular integrals, including derivatives, are computed efficiently using the effective anomaly from Eq. (B8) and the associated integration trick. Let us finally emphasise that, while Eq. (B5) is a complicated function to compute, once evaluated, one can store pre-computed interpolation functions  $(\ell, p, q, \omega) \rightarrow N_{pq}^\ell(\omega)$ , which are then used to evaluate the dressed coupling coefficients from Eq. (D1).

In order to validate our implementation of the response matrix,

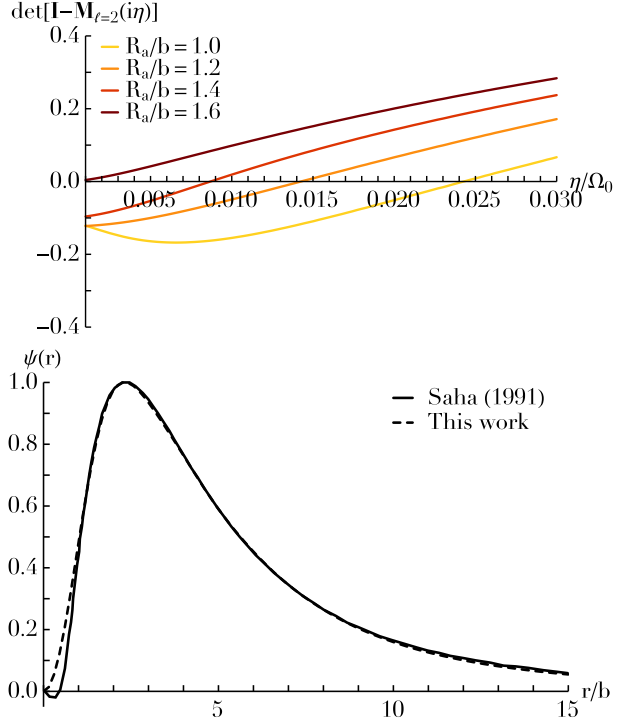


**Figure B1.** Top panel: Illustration of  $\det[\mathbf{I} - \mathbf{M}_{\ell=2}(i\eta)]$  as a function of growth rate  $\eta$ , for various values of the anisotropy radius  $R_a$ . An unstable mode is identified as soon as a curve crosses the horizontal axis. The smaller  $R_a$ , the larger the radial anisotropy, and the stronger the instability. Bottom panel: Illustration of the radial shape of the mode,  $\psi(r)$ , as measured in Fig. 4 of Saha (1991) and compared with the present method, for the unstable  $\ell=2$  mode of the  $R_a=b$  model. The normalisation of the vertical axis is arbitrary.

we set out to reproduce the radial-orbit instability of the isochrone potential recovered in Saha (1991), using the radially anisotropic DF from Eq. (F12). This is illustrated in Fig. B1. For these calculations, following Eq. (B3), we considered a total of  $n_{\max} = 20$  basis elements truncated at  $R_b = 20b$ . In Eq. (B5), the orbital integral was performed for  $\ell = 2$  using a uniform grid in  $(x, e)$ -space, with  $0 \leq x \leq x_{\max} = 10$ ,  $0 \leq e \leq 1$ , with the step distances  $\Delta x = 0.05$ , and  $\Delta e = 0.005$ , which ensures that the basis elements are never evaluated outside of their finite domain. In that same expression, the sum over resonances was limited to  $|n_1| \leq n_1^{\max} = 10$ . Finally, the orbital averages in Eq. (B6) were performed using  $K = 200$  steps in the RK4 scheme.

In Fig. B1, we recover that the model  $R_a = b$  supports an unstable mode with growth rate  $\eta \simeq 0.0245\Omega_0$  in good agreement with the value  $0.024\Omega_0$  measured in Saha (1991). In that same figure, we also illustrate the radial shape of the unstable mode, which also showed a good agreement with Saha (1991). All in all, this shows the sanity of our present numerical implementation of the response matrix.

### APPENDIX C: FOKKER-PLANCK EQUATION

In this Appendix, we detail our implementation of the orbit-averaged local diffusion coefficients that appear in the FP flux from Eq. (5). Here, we follow in particular calculations from Binney & Tremaine (2008) for the local velocity diffusion coefficients, and

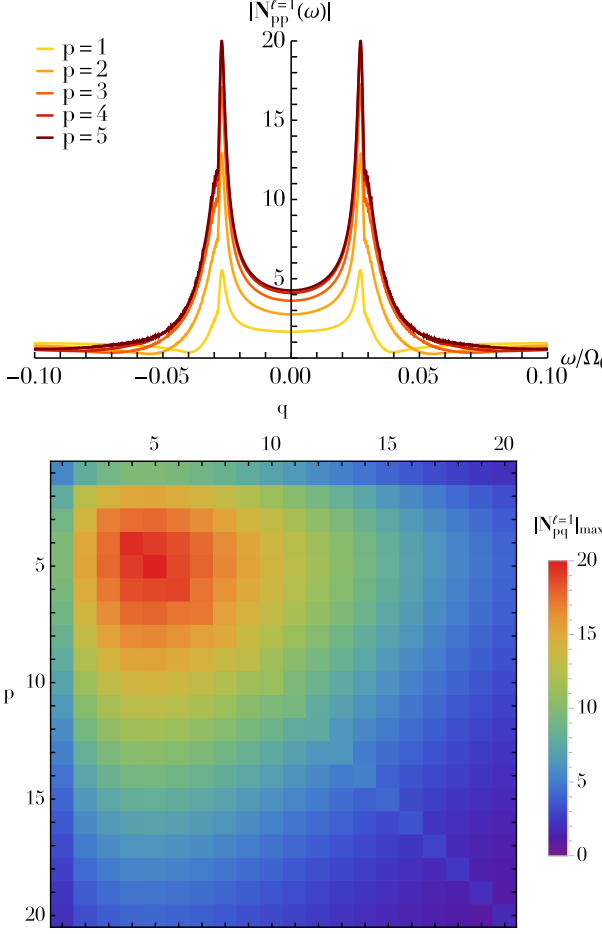


**Figure B2.** Illustration of the norm of the susceptibility matrix,  $|\mathbf{N}_\ell(\omega)|$ , for the harmonics  $\ell=1$ . *Top panel:* Norm of the diagonal coefficients,  $p=q$ , as a function of  $\omega$ . *Bottom panel:* for the whole susceptibility matrix, where the maximum norm is determined over the whole range in  $\omega$ . As already put forward in Weinberg (1994), globular clusters generically support a weakly damped  $\ell=1$  mode, located just below the real line near  $\omega/\Omega_0 \simeq 0.003$ . The BL equation accounts for the amplification of fluctuations at all real frequencies, and naturally the biggest effect is around  $\omega/\Omega_0 \simeq 0.003$ , which here leads to an efficient self-gravitating dressing of the perturbations by a factor of up to 20.

from Bar-Or & Alexander (2016) for the computation of the orbit-average.

Following Eq. (7.69) of Binney & Tremaine (2008), we write the traditional Fokker-Planck in velocity space with the convention

$$\begin{aligned} \frac{\partial P(\mathbf{v})}{\partial t} = & - \sum_{i=1}^3 \frac{\partial}{\partial v_i} [\langle \delta v_i \rangle P(\mathbf{v})] \\ & + \frac{1}{2} \sum_{i,j=1}^3 \frac{\partial^2}{\partial v_i \partial v_j} [\langle \delta v_i \delta v_j \rangle P(\mathbf{v})], \end{aligned} \quad (\text{C1})$$

where  $P(\mathbf{v})$  stands for an arbitrary DF, proportional to the number of particles within the volume  $d\mathbf{v}$ .

The first- and second-order diffusion coefficients originate from local deflections. Following Eq. (7.83a) of Binney & Tremaine (2008), and paying a careful attention to our normali-

sation convention, they read

$$\begin{aligned} \langle \delta v_i \rangle &= 8\pi G^2 \mu \ln \Lambda \frac{\partial h}{\partial v_i}, \\ \langle \delta v_i \delta v_j \rangle &= 4\pi G^2 \mu \ln \Lambda \frac{\partial^2 g}{\partial v_i \partial v_j}, \end{aligned} \quad (\text{C2})$$

where we introduced  $\ln \Lambda$  as the Coulomb logarithm. In that expression, the Rosenbluth potentials are given by

$$\begin{aligned} h(\mathbf{r}, \mathbf{v}) &= \int d\mathbf{v}' \frac{F_{\text{tot}}(\mathbf{r}, \mathbf{v}')}{|\mathbf{v} - \mathbf{v}'|}, \\ g(\mathbf{r}, \mathbf{v}) &= \int d\mathbf{v}' F_{\text{tot}}(\mathbf{r}, \mathbf{v}') |\mathbf{v} - \mathbf{v}'|. \end{aligned} \quad (\text{C3})$$

For an isotropic DF,  $F_{\text{tot}}(\mathbf{r}, \mathbf{v}) = F(r, v)$ , the diffusion coefficients are characterised by only three quantities, namely

$$\begin{aligned} \langle \delta v_{\parallel} \rangle &= -2\kappa \int_0^v dv' \frac{v'^2}{v^2} F_{\text{tot}}(v'), \\ \langle (\delta v_{\parallel})^2 \rangle &= \frac{2}{3} \kappa \left[ \int_0^v dv' \frac{v'^4}{v^3} F_{\text{tot}}(v') + \int_v^{+\infty} dv' v' F_{\text{tot}}(v') \right], \\ \langle (\delta v_{\perp})^2 \rangle &= \frac{2}{3} \kappa \left[ \int_0^v dv' \left( \frac{3v'^2}{v} - \frac{v'^4}{v^3} \right) F_{\text{tot}}(v') + 2 \int_v^{+\infty} dv' v' F_{\text{tot}}(v') \right]. \end{aligned} \quad (\text{C4})$$

where we introduced  $\kappa = 16\pi^2 G^2 \mu \ln \Lambda$ . In practice, the Coulomb logarithm is fixed following the prescription from Eq. (7).

Fortunately, in the case of an isotropic DF, we can rewrite all these integrals as integrals over the energy. Noting that  $v dv = dE$ , we can rewrite Eq. (C4) as

$$\begin{aligned} \langle \delta v_{\parallel} \rangle &= -2\kappa \frac{1}{v} I_1^{\text{inf}}, \\ \langle (\delta v_{\parallel})^2 \rangle &= \frac{2}{3} \kappa \left[ I_3^{\text{inf}} + I_0^{\text{sup}} \right], \\ \langle (\delta v_{\perp})^2 \rangle &= \frac{2}{3} \kappa \left[ 3I_1^{\text{inf}} - I_3^{\text{inf}} + 2I_0^{\text{sup}} \right], \end{aligned} \quad (\text{C5})$$

where we introduced the one-dimensional integrals

$$\begin{aligned} I_k^{\text{inf}}(r, v) &= \int_{\psi}^E dE' (v'/v)^k F_{\text{tot}}(E'), \\ I_k^{\text{sup}}(r, v) &= \int_E^0 dE' (v'/v)^k F_{\text{tot}}(E'). \end{aligned} \quad (\text{C6})$$

In these expression, the boundary of the integrals are given by  $\psi = \psi(r)$  and  $E = \frac{1}{2}v^2 + \psi(r)$ . We also note that all orbits are taken to be bound, so that  $E, E' < 0$ . In practice, these integrals are computed using the trapezoidal rule with  $K = 10^3$  steps.

From these local diffusion coefficients in velocity, we can now compute the local diffusion coefficients in  $(E, L)$ . To do so, we rely on the relations  $E = \frac{1}{2}v^2 + \psi(r)$ , and  $L = |\mathbf{r} \times \mathbf{v}|$ , that are perturbed to first order. Following Eqs. (85)–(89) in Bar-Or & Alexander (2016), we obtain

$$\begin{aligned} \langle \delta E \rangle &= v \langle \delta v_{\parallel} \rangle + \frac{1}{2} \langle (\delta v_{\parallel})^2 \rangle + \frac{1}{2} \langle (\delta v_{\perp})^2 \rangle, \\ \langle \delta L \rangle &= \frac{L}{v} \langle \delta v_{\parallel} \rangle + \frac{r^2}{4L} \langle (\delta v_{\perp})^2 \rangle, \\ \langle (\delta E)^2 \rangle &= v^2 \langle (\delta v_{\parallel})^2 \rangle, \\ \langle \delta E \delta L \rangle &= L \langle (\delta v_{\parallel})^2 \rangle, \\ \langle (\delta L)^2 \rangle &= \frac{L^2}{v^2} \langle (\delta v_{\parallel})^2 \rangle + \frac{1}{2} \left( r^2 - \frac{L^2}{v^2} \right) \langle (\delta v_{\perp})^2 \rangle. \end{aligned} \quad (\text{C7})$$

Having computed the local diffusion coefficients in  $(E, L)$ ,

we can now compute their orbit-average. For an isotropic system, it is given by the simple calculation

$$\langle \Delta E \rangle = \int_0^{\pi} \frac{d\theta_1}{\pi} \langle \delta E \rangle. \quad (C8)$$

In practice, to avoid any boundary issues, we use the exact same technique as in Eq. (B9), and introduce an effective anomaly to perform the orbit-average. In practice, these integrals are computed using a trapezoidal rule with  $K=10^3$  steps.

At this stage, we have derived the orbit-averaged diffusion coefficients in  $(E, L)$ -space. It now only remains to translate in the  $\mathbf{J}=(J_r, L)$ . Following Eqs. (122) and (123) of Bar-Or & Alexander (2016), under a coordinate transform of the form  $\mathbf{x}'=\mathbf{x}'(\mathbf{x})$ , the new diffusion coefficients are given by

$$\begin{aligned} \langle \Delta x'_k \rangle &= \frac{\partial x'_k}{\partial x_i} \langle \Delta x_i \rangle + \frac{1}{2} \frac{\partial^2 x'_k}{\partial x_i \partial x_j} \langle \Delta x_i \Delta x_j \rangle, \\ \langle \Delta x'_k \Delta x'_l \rangle &= \frac{\partial x'_k}{\partial x_i} \frac{\partial x'_l}{\partial x_j} \langle \Delta x_i \Delta x_j \rangle, \end{aligned} \quad (C9)$$

where the sums over  $i$  and  $j$  are implied. Fortunately, in the case of the isochrone potential, we have at our disposal an explicit expression for  $J_r=J_r(E, L)$ , as in Eq. (F3), which greatly eases this change of coordinates. Following all these manipulations, we finally obtain the first-order diffusion coefficient,  $\mathbf{D}_1(\mathbf{J})$ , and the second-order diffusion tensor,  $\mathbf{D}_2(\mathbf{J})$  as in equation (5).

## APPENDIX D: COMPUTING THE BALESCU-LENARD FLUX

In this Appendix we detail our computation of the inhomogeneous BL flux for spherical systems.

### D1 Dressed coupling coefficients

As already emphasised in Eq. (12), the resonant diffusion flux involves the dressed coupling coefficients,  $\Lambda_{\mathbf{n}\mathbf{n}'}^\ell(\mathbf{J}, \mathbf{J}', \omega)$ . Following Eq. (41) of Hamilton et al. (2018), they read

$$\Lambda_{\mathbf{n}\mathbf{n}'}^\ell(\mathbf{J}, \mathbf{J}', \omega) = y_\ell^{n_2} y_{\ell'}^{n'_2} \sum_{p,q} W_{\ell p}^{\mathbf{n}}(\mathbf{J}) N_{pq}^\ell(\omega) W_{\ell q}^{\mathbf{n}'}(\mathbf{J}'). \quad (D1)$$

This expression involves the in-plane coupling coefficients,  $W_{\ell n}^{\mathbf{n}}(\mathbf{J})$ , introduced in Eq. (B6). Let us also emphasise that these coefficients involve the susceptibility matrix,  $\mathbf{N}_\ell(\omega)$ , already presented in Eq. (B7), so that the pairwise coupling is said to be dressed by collective effects. Owing to the presence of the prefactor  $y_\ell^n = Y_\ell^n(\frac{\pi}{2}, 0)$ , these coefficients are non-zero only for  $|n|, |n'| \leq \ell$ , in conjunction with  $(\ell - n)$  and  $(\ell - n')$  both even.

### D2 Resonance condition

In order to compute the resonant diffusion flux from Eq. (12), one must solve the resonance condition  $\mathbf{n} \cdot \boldsymbol{\Omega} = \mathbf{n}' \cdot \boldsymbol{\Omega}'$ , with the shortened notation  $\boldsymbol{\Omega}=\boldsymbol{\Omega}(\mathbf{J})$  and  $\boldsymbol{\Omega}'=\boldsymbol{\Omega}(\mathbf{J}')$ . In order to ease that calculation, we rewrite the integral from Eq. (12) as

$$\begin{aligned} \mathcal{F}_{\mathbf{n}\mathbf{n}'}^\ell &= \int d\mathbf{J}' G(\mathbf{J}') \delta_D(\mathbf{n} \cdot \boldsymbol{\Omega} - \mathbf{n}' \cdot \boldsymbol{\Omega}') \\ &= \int dx' de' \frac{G}{\Omega_1} \left| \frac{\partial(E', L')}{\partial(x', e')} \right| \delta_D(\mathbf{n} \cdot \boldsymbol{\Omega} - \mathbf{n}' \cdot \boldsymbol{\Omega}') \\ &= \int_\gamma d\sigma(x', e') \frac{G}{\Omega_1} \left| \frac{\partial(E', L')}{\partial(x', e')} \right| \frac{1}{|\partial(\mathbf{n}' \cdot \boldsymbol{\Omega}')/\partial(x', e')|}, \end{aligned} \quad (D2)$$

where the function  $G(\mathbf{J}')$  directly follows from Eq. (12). In the second line, we used  $(x, e)=(a/b, e)$  as our orbital coordinates, following Eq. (A6), while the Jacobian of the transformation  $(E', L') \rightarrow (x', e')$  can be obtained from Eq. (A6). One interest of such a writing is that, given that  $x, e$  are both dimensionless, it is straightforward to integrate along the resonant line in these coordinates. This is highlighted in the third line of Eq. (D2), we introduced the resonant line  $\gamma$  as the 1D line in  $(x', e')$  space along which the resonance condition  $\mathbf{n}' \cdot \boldsymbol{\Omega}' = \mathbf{n} \cdot \boldsymbol{\Omega}$  is satisfied, with the associated measure  $d\sigma$ . In that expression, we also introduced the quantity  $|\partial(\omega)/\partial(x', e')| = \sqrt{(\partial\omega/\partial x')^2 + (\partial\omega/\partial e')^2}$ .

In practice, in order to estimate the integral from Eq. (D2), we must then approximate the resonance line  $\gamma$ . Examples of resonant lines are given in Fig. F1. This is done by determining a set  $\{x'_i, e'_i\}_{1 \leq i \leq Q}$  of resonance locations along the line, with  $Q \gg 1$ . We detail in Appendix F how such a search can be efficiently made in the case of the isochrone potential. We then simply replace the integral from Eq. (D2), with  $Q-1$  straight lines connecting the points. As such, we perform an estimation of the form

$$\int_\gamma d\sigma' g(x', e') \simeq \sum_{i=1}^{Q-1} g(\bar{x}'_i, \bar{e}'_i) \Delta\sigma'_i, \quad (D3)$$

where we introduced the central location  $(\bar{x}'_i, \bar{e}'_i)$  and length  $\Delta\sigma'_i$  as

$$\begin{aligned} (\bar{x}'_i, \bar{e}'_i) &= \left( \frac{1}{2}(x'_i + x'_{i+1}), \frac{1}{2}(e'_i + e'_{i+1}) \right), \\ \Delta\sigma'_i &= \sqrt{(x'_{i+1} - x'_i)^2 + (e'_{i+1} - e'_i)^2}. \end{aligned} \quad (D4)$$

Given the numerical difficulty of these calculations, it is important to limit as much as possible the number of resonance pairs to consider.

First, we note that resonance pairs with  $\mathbf{n}=(0, 0)$  or  $\mathbf{n}'=(0, 0)$  do not contribute to the diffusion, so that we limit our consideration only to the pairs such that  $\mathbf{n} \neq (0, 0)$  and  $\mathbf{n}' \neq (0, 0)$ . Glancing back at Eq. (12), we note that the resonance pairs  $(\mathbf{n}, \mathbf{n}')$  and  $(-\mathbf{n}, -\mathbf{n}')$  source the exact same flux. As a consequence, we may account for only one of the two, and add an overall factor 2 to the flux. For a given resonance vector  $\mathbf{n}$ , the associated resonance frequency is equal to  $\mathbf{n} \cdot \boldsymbol{\Omega} = \Omega_1(n_1 + \eta n_2)$ , where we followed the notation from Eq. (F6), introducing the ratio  $\eta = \Omega_2/\Omega_1$ . In the case of an outward decreasing cored density profile as the isochrone potential, one generically has  $\frac{1}{2} \leq \eta \leq 1$ . As such, simply by computing the two values  $(n_1 + \frac{1}{2}n_2)$  and  $(n_1 + n_2)$ , one can determine whether the function  $\mathbf{J} \mapsto \mathbf{n} \cdot \boldsymbol{\Omega}(\mathbf{J})$  is always positive, always negative, or changes sign. Owing to simple criterion, we can finally keep only resonance pairs  $(\mathbf{n}, \mathbf{n}')$  for which the resonance condition has a chance of being satisfied given these sign constraints.

## APPENDIX E: COMPUTING THE LANDAU FLUX

When collective effects are neglected, the BL flux becomes the Landau flux. This allows us to accelerate greatly the computation, as we now detail.

### E1 Bare coupling coefficients

Switching off collective effects at harmonic  $\ell$  is equivalent to setting the response matrix  $\mathbf{M}_\ell = 0$ . Then the coefficients  $\Lambda_{\mathbf{n}\mathbf{n}'}^\ell$ , from Eq. (D1) become independent of the temporal frequency  $\omega$  and read

$$\Lambda_{\mathbf{nn}'}^{\ell}(\mathbf{J}, \mathbf{J}') = y_{\ell}^{n_2} y_{\ell'}^{n'_2} \sum_n W_{\ell n}^{\mathbf{n}}(\mathbf{J}) W_{\ell n'}^{\mathbf{n}'}(\mathbf{J}'). \quad (\text{E1})$$

These simplified coefficients can now be computed without resorting to any biorthogonal basis. Indeed, introducing the basis elements generically amounts to assuming that the gravitational pairwise interaction,  $U(\mathbf{r}, \mathbf{r}') = -G/|\mathbf{r} - \mathbf{r}'|$ , can be decomposed under the separable form

$$\begin{aligned} U(\mathbf{r}, \mathbf{r}') &= - \sum_p \psi^{(\alpha)}(\mathbf{r}) \psi^{(\alpha)*}(\mathbf{r}') \\ &= - \sum_{\ell, m, n} Y_{\ell}^m(\hat{\mathbf{r}}) Y_{\ell}^{m*}(\hat{\mathbf{r}}') U_{\ell}^{\ell}(r) U_{\ell}^{\ell}(r'). \end{aligned} \quad (\text{E2})$$

Fortunately, using the Legendre expansion of the Newtonian interaction kernel, as well as the addition theorem for spherical harmonics, Eq. (E2) can also be rewritten as

$$U(\mathbf{r}, \mathbf{r}') = - \sum_{\ell, m} Y_{\ell}^m(\hat{\mathbf{r}}) Y_{\ell}^{m*}(\hat{\mathbf{r}}') U_{\ell}(r, r'), \quad (\text{E3})$$

where we introduced the function

$$U_{\ell}(r, r') = \frac{4\pi G}{2\ell + 1} \frac{\text{Min}[r, r']^{\ell}}{\text{Max}[r, r']^{\ell+1}}. \quad (\text{E4})$$

In the limit where collective effects can be neglected, i.e. the limit  $\mathbf{N}_{\ell}(\omega) \rightarrow \mathbf{I}$ , the dressed coupling coefficients from Eq. (D1) then naturally become

$$\Lambda_{\mathbf{nn}'}^{\ell}(\mathbf{J}, \mathbf{J}') = y_{\ell}^{n_2} y_{\ell'}^{n'_2} W_{\ell}^{\mathbf{nn}'}(\mathbf{J}, \mathbf{J}'), \quad (\text{E5})$$

where we introduced the coefficients,  $W_{\ell}^{\mathbf{nn}'}(\mathbf{J}, \mathbf{J}')$ , as

$$\begin{aligned} W_{\ell}^{\mathbf{nn}'}(\mathbf{J}, \mathbf{J}') &= \int_0^{\pi} \frac{d\theta_1}{\pi} \frac{d\theta'_1}{\pi} U_{\ell}(r, r') \\ &\times \cos(n_1 \theta_1 + n_2(\theta_2 - \psi)) \cos(n'_1 \theta'_1 + n'_2(\theta'_2 - \psi')). \end{aligned} \quad (\text{E6})$$

This seems repetitive – can be shortened significantly. Also, I found this a very confusing notation given the use of  $W$  for the dressed coefficients above. Perhaps  $w$  would be better for the bare coefficients? One of the drawbacks of such an expression is that the expression of  $W_{\ell}^{\mathbf{nn}'}(\mathbf{J}, \mathbf{J}')$  is not separable anymore, compared to Eq. (D1) where both angular averages are separated. Fortunately, in the case of the Newtonian interaction potential, such coefficients can still be computed efficiently using a traditional multipole approach, owing to the (almost) separable form of the integrand from Eq. (E6). We briefly detail this method in section E4.

## E2 Convergence of the basis function expansion

I think this doesn't really fit here but I'm not sure where to put it

In Fig. E1, we briefly discuss the errors in the coupling coefficients,  $\Lambda_{\mathbf{nn}'}^{\ell}$ , introduced by the finite truncation of the basis expansion. In particular, we note that for quasi-circular orbits, the bare coupling coefficients are affected by (very) significant errors associated with the finite truncation of the number of basis elements.

Let us now detail how one may mitigate these errors when computing the dressed coupling coefficients as defined in Eq. (D1). We assume that  $\mathbf{N}(\omega) \rightarrow \mathbf{I}$ , for  $p, q \geq n_{\text{cut}}$ , and compute the full susceptibility matrix,  $\mathbf{N}(\omega)$  only for  $1 \leq p, q \leq n_{\text{cut}}$ . Then for the remaining  $p, q > n_{\text{cut}}$  we use the bare coefficients, so that Eq. (D1)

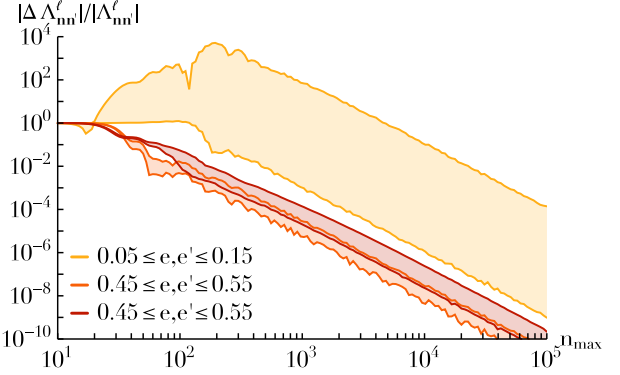


**Figure E1.** Illustration of the relative errors in the bare coupling coefficient,  $\Lambda_{\mathbf{nn}'}^{\ell}(\mathbf{J}, \mathbf{J}')$ , using the basis method as in Eq. (E1) vs. the multipole expression from Eq. (E5), as a function of the total number of basis elements. Following Eq. (B9), the angular integrals were performed using  $K = 10^5$  steps, with  $\ell = 1$ ,  $\mathbf{n} = (2, 1)$  and  $\mathbf{n}' = (3, 1)$ , and a potential basis satisfying  $R_b = 20 \times b$ . We considered  $10^4$  pairs of orbits with  $x = 1.0$  and  $x' = 1.2$ , with the associated eccentricities,  $e$  and  $e'$ , taken uniformly within some finite range. Colored regions correspond to the 16% and 84% levels among the pairs of orbits. We note in particular that the basis method converges significantly more slowly for quasi-circular orbits. **This means that the number of basis elements used in H18 was way too small – discuss either here or in Discussion**

becomes

$$\begin{aligned} \Lambda_{\mathbf{nn}'}^{\ell}(\mathbf{J}, \mathbf{J}', \omega) &= y_{\ell}^{n_2} y_{\ell'}^{n'_2} \left\{ \sum_{p, q=1}^{n_{\text{cut}}} W_{\ell p}^{\mathbf{n}}(\mathbf{J}) N_{pq}(\omega) W_{\ell q}^{\mathbf{n}'}(\mathbf{J}') \right. \\ &\quad \left. + \sum_{p=n_{\text{cut}}+1}^{+\infty} W_{\ell p}^{\mathbf{n}}(\mathbf{J}) W_{\ell p}^{\mathbf{n}'}(\mathbf{J}') \right\}, \end{aligned} \quad (\text{E7})$$

where we introduced the shortened notation  $W_p = W_{\ell n}^{\mathbf{n}}(\mathbf{J})$ , and similarly for  $W'_q$ . Using (E1) this can be rewritten as

$$\begin{aligned} \Lambda_{\mathbf{nn}'}^{\ell}(\mathbf{J}, \mathbf{J}', \omega) &= y_{\ell}^{n_2} y_{\ell'}^{n'_2} \left\{ \sum_{p, q=1}^{n_{\text{cut}}} W_{\ell p}^{\mathbf{n}}(\mathbf{J}) [N_{pq}(\omega) - \delta_{pq}] W_{\ell q}^{\mathbf{n}'}(\mathbf{J}') \right. \\ &\quad \left. + W_{\ell}^{\mathbf{nn}'}(\mathbf{J}, \mathbf{J}') \right\}, \end{aligned} \quad (\text{E8})$$

where, importantly, the last term is obtained through the multipole expression from Eq. (E6), that does not require any basis elements.

## E3 Softened bare coupling coefficients

It is also possible to obtain the bare coupling coefficients associated with a softened pairwise interaction of the form

$$U(\mathbf{r}, \mathbf{r}', \varepsilon) = - \frac{G}{\sqrt{|\mathbf{r} - \mathbf{r}'|^2 + \varepsilon^2}}, \quad (\text{E9})$$

with  $\varepsilon$  the considered softening length. Following Appendix B of Weinberg (1986), (see also Wachlin & Carpintero (2006)), in the softened case, Eq. (E4) becomes

$$U_{\ell}(r, r', \varepsilon) = \frac{4\pi G}{2\ell + 1} \frac{r_{\beta}^{\ell}}{r_{\alpha}^{\ell+1}}, \quad (\text{E10})$$

where we introduced the notations

$$r_\alpha = \left[ \frac{1}{2} \left( r^2 + r'^2 + \varepsilon^2 + \sqrt{((r+r')^2 + \varepsilon^2)((r-r')^2 + \varepsilon^2)} \right) \right]^{1/2},$$

$$r_\beta = \frac{r r'}{r_\alpha}. \quad (\text{E11})$$

From Eq. (E11), one can immediately recover the unsoftened limit from Eq. (E4). Unfortunately, the expression from Eq. (E10) is far from being (almost) separable, so that it cannot benefit from the fast evaluation permitted by the multipole approach, as we will now detail.

Let us already note that, even for the softened interaction kernel from Eq. (E10), we can perform the same asymptotic expansion as in Eq. (13), see Eq. (B8) of Weinberg (1986). As such, let us assume that  $r=b$ ,  $r'=b(1-\alpha)$ , with  $\alpha > 0$ . Assuming that  $\mathcal{O}(\alpha) \simeq \mathcal{O}(\varepsilon)$ , one can write the following expansions

$$r_\alpha \simeq b + \mathcal{O}(\varepsilon),$$

$$\frac{r_\beta}{r_\alpha} \simeq 1 - \sqrt{\alpha^2 + (\varepsilon/b)^2} + \mathcal{O}(\varepsilon^2). \quad (\text{E12})$$

As a consequence, in the limit  $\alpha, \varepsilon \ll 1$  and  $\ell \geq 1$ , we can expand Eq. (E10) as

$$U_\ell(\alpha) \propto \frac{1}{b} (1 - \sqrt{\alpha^2 + (\varepsilon/b)^2})^\ell$$

$$\simeq \frac{1}{b} e^{-\ell \sqrt{\alpha^2 + (\varepsilon/b)^2}}. \quad (\text{E13})$$

This is the direct equivalent of Eq. (14) in the case of a softened interaction. In particular, we note that for interparticle separations,  $\alpha$ , smaller than the softening length,  $\varepsilon$ , the pairwise coupling tends to a constant value, which, in essence, turns off the ability to sustain any relaxation on such small scale.

#### E4 Multipole expansion

Let us now briefly detail how the unsoftened bare coupling coefficients from Eq. (E6) using a multipole approach. First, in order not to have to invert the implicit relation  $\theta_1 = \theta_1(r)$  (see Eq. (A3)), and to avoid boundary divergences at the edge of the integration domain where the radial velocity vanishes, we rely on the same effective anomaly,  $r=r(u)$ , as in Eq. (B8). Equation (E6) then becomes

$$W_\ell^{\text{nn}'}(\mathbf{J}, \mathbf{J}') = \frac{4}{\pi^2} \int_{-1}^1 \frac{du}{2} \frac{du'}{2} g(r) g'(r') U_\ell(r, r'), \quad (\text{E14})$$

where we introduced the function

$$g(r) = \frac{d\theta_1}{dr} \frac{dr}{du} \cos(n_1 \theta_1 + n_2(\theta_2 - \psi)), \quad (\text{E15})$$

and similarly for  $g'(r')$ .

To perform the two integrals from Eq. (E14), we now sample uniformly each interval using  $K$  nodes. Specifically, for  $1 \leq j \leq K$ , we sample the anomaly  $u$  with

$$u_k = \Delta u \left( k - \frac{1}{2} \right) \quad \text{with} \quad \Delta u = \frac{2}{K}. \quad (\text{E16})$$

Following this discretisation, Eq. (E14) becomes

$$W_\ell^{\text{nn}'} = \frac{16G}{\pi(2\ell+1)} \frac{1}{K^2} \sum_{i,j} g_i g'_j \frac{\text{Min}[r_i, r'_j]^\ell}{\text{Max}[r_i, r'_j]^{\ell+1}}, \quad (\text{E17})$$

where we used the shortened notation  $g_i = g(r_i)$ .

Let us now use the particular structure of Eq. (E17) to accelerate its evaluation. To proceed forward, we order the set of radii

$\{r_i, r'_j\}$  by increasing order. Let us emphasise that this can be made in  $\mathcal{O}(K)$  steps, as the two sets  $\{r_i\}$  and  $\{r'_j\}$  are already ordered, so that it only remains to merge the two lists. Following this ordering, we construct the array  $w_j$  which, for  $1 \leq j \leq K$ , is defined as

$$w_j = \text{Card} \left\{ i \in \{1, \dots, K\} \mid r_i \leq r'_j \right\}, \quad (\text{E18})$$

(It might be possible to rewrite these sums without introducing  $w$ , so as to simplify the notations?) with the boundary terms  $w_0 = 0$  and  $w_{K+1} = K$ . We can now rewrite the double sum from Eq. (E17) as

$$W_\ell^{\text{nn}'} = \frac{16G}{\pi(2\ell+1)} \frac{1}{K^2} \sum_{j=1}^K g'_j [P_j + Q_j], \quad (\text{E19})$$

where we introduced

$$P_j = \sum_{i=1}^{w_j} g_i \frac{r_i^\ell}{r_j^{\ell+1}}; \quad Q_j = \sum_{i=w_j+1}^K g_i \frac{r_i^{\ell+1}}{r_j^\ell}. \quad (\text{E20})$$

Here, it is essential to note that both  $P_j$  and  $Q_j$  can be computed with a complexity scaling linearly with  $K$ . To highlight, let us define for  $1 \leq j \leq K$ , the partial sums

$$\delta P_j = \sum_{i=w_{j-1}+1}^{w_j} g_i \frac{r_i^\ell}{r_j^{\ell+1}}; \quad \delta Q_j = \sum_{i=w_j+1}^{w_{j+1}} g_i \frac{r_i^{\ell+1}}{r_j^\ell}, \quad (\text{E21})$$

which satisfy the recurrence relations

$$P_1 = \delta P_1; \quad P_{j+1} = \left[ \frac{r'_j}{r'_{j+1}} \right]^{\ell+1} P_j + \delta P_{j+1},$$

$$Q_K = \delta Q_K; \quad Q_{j-1} = \left[ \frac{r'_{j-1}}{r'_j} \right]^\ell Q_j + \delta Q_{j-1}. \quad (\text{E22})$$

Owing to these explicit recurrence relations, we are in a position to compute the bare coupling coefficients,  $W_\ell^{\text{nn}'}(\mathbf{J}, \mathbf{J}')$ , with a complexity in  $\mathcal{O}(K)$ .

As a closing remark, let us detail a bit more the preparation of Eq. (E17). In that equation, one must compute  $\theta_1[u_k]$  and  $(\theta_2 - \psi)[u_k]$ . This is done using the same method as in Eq. (B9), i.e. by a RK4 integration of each expression. In practice, the initial value of the various integrals are obtained through a first ‘warm-up’ starting from  $u = -1$  with one RK4 step of length  $du/2$ .

#### APPENDIX F: ISOCHRONE POTENTIAL

In this section, we follow Hénon (1959), and recall some of the key analytical expressions of the isochrone potential, that will be used throughout the paper. It is defined as

$$\psi(r) = -\frac{GM}{b + \sqrt{b^2 + r^2}}, \quad (\text{F1})$$

with  $M$  the system’s total active mass, and  $b$  its lengthscale. In practice, for all the numerical applications, we pick units so that  $G = M = b = 1$ . The isochrone Hamiltonian can be explicitly written as a function of the action coordinates. It reads

$$H(\mathbf{J}) = -\frac{(GM)^2}{2[J_r + \frac{1}{2}(L + \sqrt{L^2 + 4GMb})]}. \quad (\text{F2})$$

Fortunately, that same expression also provides with an explicit inversion of the expression of the radial action, so that

$$J_r = \frac{GM}{\sqrt{-2E}} - \frac{1}{2} \left( L + \sqrt{L^2 + 4GMb} \right). \quad (\text{F3})$$

The radial frequency is given by

$$\Omega_1 = \omega(a, e) \Omega_0, \quad (\text{F4})$$

with the frequency scale  $\Omega_0 = \sqrt{GM/b^3}$ . In Eq. (F4), we introduced the dimensionless function

$$\omega(a, e) = \left( \frac{E}{E_{\min}} \right)^{3/2} = \left( \frac{2}{s_p + s_a} \right)^{3/2}, \quad (\text{F5})$$

where we introduced  $s_p = \sqrt{1+x_p^2}$  (similarly for  $s_a$ ) with the dimensionless pericentre  $x_p = r_p/b$ , as well as the minimum energy  $E_{\min} = -GM/(2b)$ . The azimuthal frequency is given by

$$\Omega_2 = \omega(a, e) \eta(a, e) \Omega_0, \quad (\text{F6})$$

where we introduced the frequency ratio  $\eta = \Omega_2/\Omega_1$ . In the isochrone case, it follows the explicit form

$$\begin{aligned} \eta(a, e) &= \frac{1}{2} \left( 1 + \frac{L}{\sqrt{L^2 + 4GMb}} \right) \\ &= \frac{1}{2} \left( 1 + \frac{x_p x_a}{(1+s_p)(1+s_a)} \right). \end{aligned} \quad (\text{F7})$$

We note that along circular (resp. radial) orbits, i.e. for  $e \rightarrow 0$  (resp.  $e \rightarrow 1$ ), the isochrone frequencies take the simple forms

$$\begin{cases} \omega_{\text{circ}}(x) = \left( \frac{1}{\sqrt{1+x^2}} \right)^{3/2}, & \omega_{\text{rad}}(x) = \left( \frac{2}{1+\sqrt{1+4x^2}} \right)^{3/2}, \\ \eta_{\text{circ}}(x) = \frac{\sqrt{1+x^2}}{1+\sqrt{1+x^2}}, & \eta_{\text{rad}}(x) = \frac{1}{2}. \end{cases} \quad (\text{F8})$$

In the specific case of the isochrone potential, one can also get numerically well-posed expressions for  $E = E(r_p, r_a)$  and  $L = L(r_p, r_a)$  from Eq. (A5). It reads

$$E = \frac{E_0}{s_p + s_a}; \quad L = \sqrt{2} L_0 \frac{x_p x_a}{\sqrt{(1+s_p)(1+s_a)(s_p+s_a)}}, \quad (\text{F9})$$

(The expression for  $L$  can be written under a shorter form.) with the energy scale  $E_0 = -GM/b$ , and the action scale  $L_0 = \sqrt{GMb}$ . These explicit expressions finally allow us to obtain exact expressions for the Jacobian  $d\theta_1/du$  appearing in Eq. (B9)

$$\frac{d\theta_1}{du} = \frac{3}{\sqrt{2}} \frac{\Omega_1}{\Omega_0} \frac{x_r}{\sqrt{4-u^2}} \frac{\sqrt{(s_r+s_p)(s_r+s_a)(s_p+s_a)}}{\sqrt{(x_r+x_p)(x_r+x_a)}}, \quad (\text{F10})$$

where we introduced  $x_r = r/b$ , and  $s_r = \sqrt{1+x_r^2}$ . Importantly, we note that this expression is numerically well-behaving for any  $-1 \leq u \leq u$ .

Following Eq. (4.54) of Binney & Tremaine (2008), the isotropic DF of the isochrone potential reads

$$\begin{aligned} F_{\text{tot}}(E) &= \frac{M}{(GMb)^{3/2}} \frac{1}{128\sqrt{2}\pi^3} \frac{\sqrt{\mathcal{E}}}{(1-\mathcal{E})^4} \\ &\times \left[ 27 - 66\mathcal{E} + 320\mathcal{E}^2 - 240\mathcal{E}^3 + 64\mathcal{E}^4 \right. \\ &\left. + \frac{3\sin^{-1}(\sqrt{\mathcal{E}})}{\sqrt{\mathcal{E}(1-\mathcal{E})}} (-9 + 28\mathcal{E} + 16\mathcal{E}^2) \right]. \end{aligned} \quad (\text{F11})$$

where we introduced the rescaled energy  $\mathcal{E} = E/E_0$ . Owing to Eq. (F11), one can compute all the gradients  $\partial F/\partial \mathbf{J}$  that appear both in the response matrix from Eq. (B5) and in the BL diffusion flux from Eq. (12).

In Appendix B3, we validate our implementation of the response matrix by recovering the radial orbit instability in a radially

anisotropic isochrone cluster following Saha (1991). In that case, we consider an anisotropic DF defined as

$$\begin{aligned} F_{\text{tot}}(Q) &= \frac{M}{(GMb)^{3/2}} \frac{1}{128\sqrt{2}\pi^3} \frac{\sqrt{Q}}{(1-Q)^4} \\ &\times \left\{ 27 + 77\gamma - (66 + 286\gamma)Q + (320 + 136\gamma)Q^2 \right. \\ &\left. - (240 + 32\gamma)Q^3 + 64Q^4 \right. \\ &\left. + \frac{3\sin^{-1}(\sqrt{Q})}{\sqrt{Q(1-Q)}} [(-9 + 17\gamma) + (28 - 44\gamma)Q + (16 - 8\gamma)Q^2] \right\}, \end{aligned} \quad (\text{F12})$$

where we introduced

$$Q = \frac{1}{E_0} \left( E + \frac{L^2}{2R_a^2} \right); \quad \gamma = \left( \frac{b}{R_a} \right)^2. \quad (\text{F13})$$

Here  $R_a$  is the so-called *anisotropy radius*. Stars orbiting at radii much smaller than  $R_a$  tend to have isotropically distributed velocities while stars at radii much larger than  $R_a$  are nearly all on highly radial orbits. For  $R_a \lesssim 1.2b$  the DF  $F_{\text{tot}}(Q)$  is unstable to the  $\ell = 2$  radial orbit instability. In the limit  $R_a \rightarrow +\infty$ , one has  $Q \rightarrow \mathcal{E}$  and  $\gamma \rightarrow 0$ , so that Eq. (F12) reduces to Eq. (F11).

In order to compute the resonant flux from Eq. (12), one has to compute a resonance condition of the form  $\delta_D(\mathbf{n} \cdot \Omega(\mathbf{J}) - \mathbf{n}' \cdot \Omega(\mathbf{J}'))$ . As already defined in Eq. (D2), this amounts to finding all the resonant locations  $(x', e')$  such that the resonance condition  $\mathbf{n}' \cdot \Omega(x', e') = \mathbf{n} \cdot \Omega(\mathbf{J})$  is satisfied.

In conjunction with the computation of the response matrix, this is one of the most cumbersome task in the estimation of the dressed diffusion flux. Fortunately, such a search can be eased in the case of the isochrone potential, owing to the explicit expressions of the associated orbital frequencies recalled in Eqs. (F5) and (F7). Let us now briefly detail our scheme to construct the system's resonance lines.

Following Eq. (12), a resonance is characterised by a resonance vector  $\mathbf{n}' = (n'_1, n'_2)$ . Following Eqs. (F4) and (F6), the associated resonance condition reads

$$\omega_{\text{res}}(x', e') = \varpi, \quad (\text{F14})$$

where we introduced the resonance frequency  $\omega_{\text{res}} = \omega(n'_1 + n'_2 \eta)$ , as well as the rescaled frequency  $\varpi = \mathbf{n} \cdot \Omega(\mathbf{J})/\Omega_0$ .

First, we compute the quantity

$$\nu \equiv n'_1 + \frac{1}{2} n'_2. \quad (\text{F15})$$

Owing to the simple expression of  $\eta_{\text{rad}}$  from Eq. (F8), we have the inequality  $|\omega_{\text{res}}(x, e=1)| \leq |\nu|$ , and the function  $x' \mapsto \omega(x', e=1)$  is a monotonic function. As a consequence, dealing appropriately with the case  $\nu = 0$ , we may conclude that the resonance line goes up to the radial orbit if one has

$$0 \leq \frac{\varpi}{\nu} \leq 1. \quad (\text{F16})$$

If this constraint is satisfied, the resonance line reaches radial orbits for  $x' = x'_{\text{rad}}$  so that  $\omega_{\text{res}}(x'_{\text{rad}}, e') = \varpi$  with the explicit expression

$$x'_{\text{rad}} = \frac{\sqrt{1 - (\varpi/\nu)^{2/3}}}{(\varpi/\nu)^{2/3}}. \quad (\text{F17})$$

Having determined whether or not the resonance line reaches the radial orbits, we must now consider how it reaches the circular orbit. Along circular orbits, the resonance frequency takes the form

$$\omega_{\text{res}}(x', e'=0) = \frac{1}{q^{3/2}} \left[ n'_1 + n'_2 \frac{q}{1+q} \right] \equiv h(q), \quad (\text{F18})$$

where we introduced  $q = \sqrt{1 + x^2}$ . We note therefore that the boundary terms are given by  $\omega_{\text{res}}(x' = 0, e' = 0) = \nu$  and  $\omega_{\text{res}}(x' = +\infty, e' = 0) = 0$ . Since these are the same bounds as in Eq. (F16), we conclude that any resonance line that reaches the radial orbits necessarily reaches the circular orbits. Here, the importance difference is that the function  $q \mapsto h(q)$  might not be monotonic.

We note that we have the systematic bound  $|h(q)| \leq (|n'_1| + |n'_2|)/q^{3/2}$ , so that introducing

$$q_b = \left( \frac{2(|n'_1| + |n'_2|)}{|\varpi|} \right)^{2/3}, \quad (\text{F19})$$

one gets that  $q \leq q_b$  implies  $|h(q)| \leq |\varpi|/2$ . In the case where Eq. (F16) is satisfied, such a bound provides us with an explicit interval within which to perform a bisection search in order to obtain the location at which the resonance line intersects the circular orbits,  $x'_{\text{circ}}$ . Once  $(x'_{\text{circ}}, x'_{\text{rad}})$  have been determined, we sample uniformly the range  $0 \leq e' \leq 1$  with  $K_{\text{res}}$  points, and we use bisection searches to identify precisely the resonance locations. In practice, we also ensure that the resonant search is constrained to the domain  $0 \leq x' \leq x_{\text{max}}$ .

Even if the condition from Eq. (F16) is not met, the system can still support a resonance line that would not reach radial orbits, but would rather connect two circular orbits. To find such lines, we follow Eq. (F18) and write

$$\frac{dh}{dq} = \frac{P(q)}{2q^{5/2}(1+q)^2}, \quad (\text{F20})$$

where we introduced the second-order polynomial

$$P(q) = -3(n'_1 + n'_2)q^2 - (6n'_1 + n'_2)q - 3n'_1. \quad (\text{F21})$$

We note that if  $n'_2 = -n'_1$ ,  $P(q)$  becomes linear in  $q$ . In the range  $1 \leq q \leq +\infty$  this function is of constant sign, i.e. the function  $h(q)$  is monotonic. As a consequence, for such resonances, we may use the exact same criteria as in Eq. (F16), and all the resonance lines connect the circular orbits to the radial ones.

Let us then assume  $n'_2 \neq -n'_1$ . The polynomial  $P(q)$  from Eq. (F21) is then a true second-order polynomial, and its discriminant reads

$$\Delta = n'_2(n'_2 - 24n'_1). \quad (\text{F22})$$

If  $\Delta \leq 0$ ,  $P(q)$  does not change sign. As a consequence,  $h(q)$  is monotonic. The criteria from Eq. (F16) applies again, and all the resonance lines connect the circular orbits to the radial ones.

If  $\Delta > 0$ ,  $P(q)$  has two roots, i.e. it changes of sign. It only remains to determine whether or not this change of sign occurs within the domain  $1 \leq q < +\infty$ . The two roots of  $P(q)$  are given by

$$q_{\pm} = \frac{-(6n'_1 + n'_2) \pm \sqrt{\Delta}}{6(n'_1 + n'_2)}, \quad (\text{F23})$$

which are subsequently ordered as

$$q_{\min} = \text{Min}[q_-, q_+]; \quad q_{\max} = \text{Max}[q_-, q_+]. \quad (\text{F24})$$

It is only if  $1 < q_{\max}$  that the system can support resonance line joining two circular orbits. In that case, we use a bisection search to identify these two radii  $x'_{\min}$  and  $x'_{\max}$  where the resonance condition is met. We may then sample uniformly the range  $x'_{\min} \leq x' \leq x'_{\max}$  with  $K_{\text{res}}$  points and we use bisection searches to identify precisely the resonance locations. In practice, we also enforce that the additional constraint that the resonance line is limited to the domain  $0 \leq x' \leq x_{\text{max}}$ .

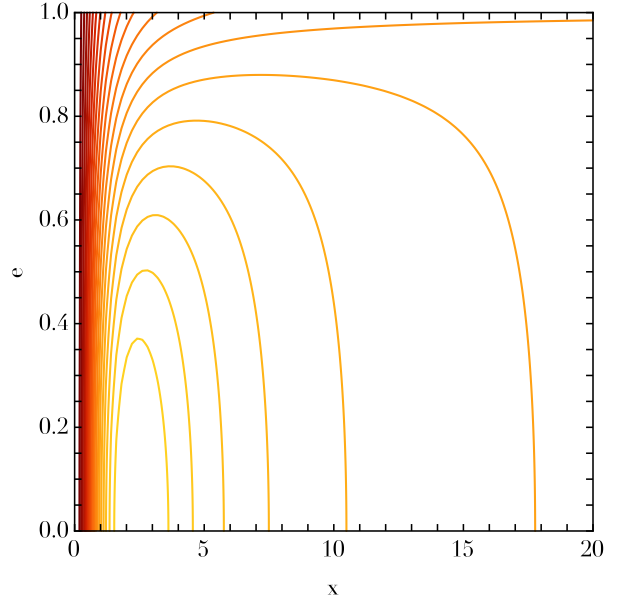


**Figure F1.** Illustration of the resonance frequency  $\omega_{\text{res}} = \mathbf{n} \cdot \boldsymbol{\Omega}(x, e)$  for an isochrone cluster, considering the resonance vector  $\mathbf{n} = (4, -7)$ . In particular, one can note that there exist two types of resonance line, depending on whether or not it reaches radial orbits ( $e = 1$ ).

To conclude this Appendix, we briefly illustrate in Fig. F1 an example of resonance lines, where one can note, as already discussed, the presence of two types of resonance lines depending on whether or not they reach radial orbits.

## APPENDIX G: NUMERICAL SIMULATIONS

In this Appendix, we briefly detail the properties of the numerical simulations. We performed two types of simulations: (i) using the (unsoftened) direct code NBODY6++GPU (Wang et al. 2015); (ii) using the (softened) collisionless code *gyrfalcon* (Dehnen 2000).

In order to ease the description of each of these setups, for this Appendix, all units are now displayed in Hénon units (HU Hénon 1971). For the isochrone potential from Eq. (F1), the virial theorem gives the system's velocity dispersion as (see, e.g., Eq. (B36) Hamilton et al. 2018)

$$\sigma^2 = \frac{GM}{b} \left( \frac{\pi}{4} - \frac{2}{3} \right). \quad (\text{G1})$$

As a result, the length-scale of the Hénon units is given by

$$r_{\text{H}} = \frac{6}{3\pi - 8} b \simeq 4.21 b. \quad (\text{G2})$$

(Detail how the actions are computed, and how  $\partial F/\partial t$  is measured.) (Detail how the recentering is performed.)

### G1 Collisional simulations

(Give the parameters of the runs.)

As in the main text, each cluster was composed of  $N = 10^5$  particles. Each individual realisation was run on a node with a single GPU and a 40-core CPU. Integrating one realisation for  $t_{\text{max}} = 10^3$  HU required about 256 of computation. We performed a total of  $N_{\text{real}} = 10^2$  different realisations.

## G2 Collisionless simulations

(Give the parameters of the runs.)

Simulations were performed using the softening kernel,  $P_0$ , whose penosity and read

(To do.) (G3)

(Please give also the expression of the associated potential, so that we could compare it with Eq. (E9).) To fix the softening length, we followed the same approach as in Theuns (1996) (see Eq. (14) therein). In the very core of the cluster, the typical interparticle distance is given by

$$d = [\mu/\rho(0)]^{1/3}. \quad (G4)$$

For the isochrone potential from Eq. (F1), (see Eq. (2.49) of Binney & Tremaine (2008) for the associated density), this simply becomes

$$\begin{aligned} d &= [16\pi/(3N)]^{1/3} b \\ &\simeq 0.055 b \quad \text{for } N = 10^5. \end{aligned} \quad (G5)$$

(here the factor is  $6/(3\pi - 8)$ ) It is then appropriate to consider a softening length comparable with this scale. In practice, we used

$$\begin{aligned} \varepsilon &= d/2 \\ &\simeq 0.028 b \quad \text{for } N = 10^5. \end{aligned} \quad (G6)$$

As in the main text, each cluster was composed of  $N = 10^5$  particles. Each individual realisation was run on a single CPU-core. Integrating one realisation for  $t_{\max} = 10^3$  HU required about 24h of computation. We performed a total of  $N_{\text{real}} = 10^2$  different realisations.